

Effects of different geometries on the conductance, shot noise and tunnel magnetoresistance of double quantum dots

Ireneusz Weymann^{1, 2, *}

¹*Department of Physics, Adam Mickiewicz University, 61-614 Poznań, Poland*

²*Department of Theoretical Physics, Institute of Physics,
Budapest University of Technology and Economics, H-1521 Budapest, Hungary*

(Dated: October 30, 2018)

The spin-polarized transport through a coherent strongly coupled double quantum dot (DQD) system is analyzed theoretically in the sequential and cotunneling regimes. Using the real-time diagrammatic technique, we analyze the current, differential conductance, shot noise and tunnel magnetoresistance (TMR) as a function of both the bias and gate voltages for double quantum dots coupled in series, in parallel as well as for T-shaped systems. For DQDs coupled in series, we find a strong dependence of the TMR on the number of electrons occupying the double dot, and super-Poissonian shot noise in the Coulomb blockade regime. In addition, for asymmetric DQDs, we analyze transport in the Pauli spin blockade regime and explain the existence of the leakage current in terms of cotunneling and spin-flip cotunneling-assisted sequential tunneling. For DQDs coupled in parallel, we show that the transport characteristics in the weak coupling regime are qualitatively similar to those of DQDs coupled in series. On the other hand, in the case of T-shaped quantum dots we predict a large super-Poissonian shot noise and TMR enhanced above the Julliere value due to increased occupation of the decoupled quantum dot. We also discuss the possibility of determining the geometry of the double dot from transport characteristics. Furthermore, where possible, we compare our results with existing experimental data on nonmagnetic systems and find qualitative agreement.

PACS numbers: 72.25.Mk, 73.63.Kv, 85.75.-d, 73.23.Hk

I. INTRODUCTION

Transport properties of double quantum dots (DQDs) have recently attracted much interest.^{1,2,3,4,5,6,7,8,9,10,11,12,13,14,15,16,17,18,19,20,21,22,23,24} Since the behavior of double quantum dots resembles the behavior of molecules, DQDs are frequently called *artificial molecules*, and are thus considered as ideal systems to study the fundamental many-body interactions between single electrons and spins.^{25,26,27,28,29} Double quantum dots exhibit a variety of interesting effects, such as for example current rectification due to the Pauli spin blockade,^{4,6,15,16,17,18} negative differential conductance,⁸ formation of molecular states,^{2,3,12} spin pumping,^{13,14} Kondo effect,^{30,31,32} etc. Furthermore, double quantum dots are also interesting for future applications in quantum computing.^{33,34,35,36} In addition, when the leads are ferromagnetic, transport properties of the system strongly depend on the relative orientation of the magnetizations of electrodes, leading to the tunnel magnetoresistance (TMR) effect, spin accumulation, exchange field, etc.^{22,23,37,38,39,40,41,42,43}

The problem of spin-polarized transport properties has been so far mainly addressed in the case of single quantum dots.^{39,40,41,42,43,44,45,46,47,48,49,50,51,52,53,54} In particular, in the strong coupling regime it was shown that the Kondo peak becomes split when the magnetic configuration changes from the antiparallel to parallel one, and that this splitting can be compensated upon applying external magnetic field.^{51,52,53} In the weak coupling regime, on the other hand, the parity effect of the linear response

TMR was predicted⁴³ and the zero-bias anomaly was found in the differential conductance when magnetic moments of the leads form an antiparallel configuration.⁴⁴ In this paper we extend the existing theoretical studies and consider transport through coherent double quantum dots weakly coupled to external ferromagnetic leads. We note that spin-dependent transport properties of DQDs have been analyzed very recently in a few theoretical papers.^{16,23,55} The considerations were however limited to either first-order tunneling or the Coulomb blockade regime. In particular, in Ref. [16] the formation of a pure triplet state was predicted, Ref. [23] deals with transport in the deep Coulomb blockade regime, while Ref. [55] presents a detailed analysis of sequential transport in the case of non-collinearly polarized leads.

The goal of this paper is thus to analyze the transport properties of double quantum dots coupled to collinear ferromagnetic leads in the full weak coupling regime, i.e. including sequential, cotunneling and cotunneling-assisted sequential processes. Furthermore, we also analyze the effect of different geometries of the double dots on transport, in particular, the cases of DQDs coupled in series, in parallel, as well as T-shaped double quantum dots are considered. The comparison of numerical results obtained for different geometries may in principle help in determining the system's geometry, which may be of importance in discussing and understanding experimental results, especially on self-assembled quantum dots. The present analysis is based on the real-time diagrammatic technique which consists in a perturbation expansion of the density matrix of the system under consideration,

and the relevant operators, with respect to the coupling to external leads. The advantage of using the real-time diagrammatic technique is that it takes into account the effects of the exchange field and the renormalization of the dot levels in a fully systematic way. In particular, in the case of asymmetric DQDs coupled in series, we consider transport in the Pauli spin blockade regime and show that the leakage current in the blockade region results from cotunneling and cotunneling-assisted sequential tunneling processes. As far as the shot noise is concerned, we show that the noise is super-Poissonian in the Coulomb blockade regime and drops to sub-Poissonian value in the sequential tunneling regime, where the Fano factor approaches one half. This behavior is observed for parallel and serial DQD's geometries. In turn, for T-shaped double quantum dots, we find a large super-Poissonian shot noise due to increased occupation of the decoupled dot. We also analyze the TMR effect and find its strong dependence on the transport regime and number of electrons in the DQD in the ground state. For DQDs coupled in series and in parallel the TMR takes the values ranging from around a half of the Julliere TMR to its full value,³⁷ whereas for T-shaped DQDs the TMR may be enhanced above the Julliere value.

The systems considered in this paper may be realized experimentally for example in lateral and vertical semiconductor quantum dots^{6,8,10,56,57} or single wall metallic carbon nanotubes with top gate electrodes.^{12,58,59,60} The latter systems are of particular interest because, by tuning the gates, it is possible to change the charge on each dot separately. Unfortunately, the aforementioned experiments concerned only DQDs coupled to nonmagnetic leads. There are several experimental realizations of single quantum dots attached to ferromagnetic leads,^{61,62,63,64,65,66,67,68,69,70,71,72,73} while experimental data on spin-polarized transport through double quantum dots are lacking. We thus believe that the results presented in this paper will be of assistance in discussing future experiments.

The paper is organized as follows: The model of the considered system is presented in Sec. II, whereas the method employed in calculations is described in Sec. III. In Section IV we present and discuss the numerical results for double quantum dots coupled in series. In this section we also focus on the role of second-order processes in transport. In addition, we also analyze transport in the Pauli spin blockade regime. In Sec. V we deal with DQDs coupled in parallel, whereas in Sec. VI we consider transport through T-shaped quantum dots. Finally, the conclusions are given in Sec. VII.

II. MODEL

The schematic of a double quantum dot coupled to ferromagnetic leads is shown in Fig. 1. It is assumed that the magnetizations of the leads are oriented collinearly, so that the system can be either in the parallel or an-

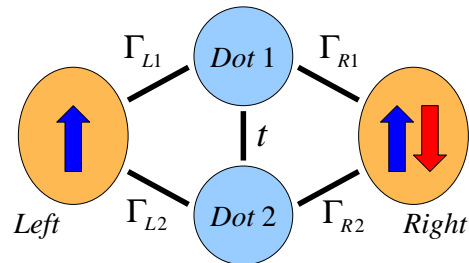


FIG. 1: (Color online) Schematic of a double quantum dot weakly coupled to external ferromagnetic electrodes. The magnetizations of the leads can form either parallel or antiparallel magnetic configuration. The first ($j = 1$) and second ($j = 2$) dots are coupled to each other via the hopping t , and to the left ($r = L$) and right ($r = R$) leads with the coupling strength Γ_{rj} . The double quantum dot is assumed to be symmetrically biased. By adjusting the couplings, the system can smoothly cross over from the serial to parallel geometry.

tiparallel magnetic configuration. The Hamiltonian of the system is given by

$$H = H_L + H_R + H_{\text{DQD}} + H_T \quad (1)$$

The first two terms describe noninteracting itinerant electrons in the leads, $H_r = \sum_{\mathbf{k}\sigma} \varepsilon_{r\mathbf{k}\sigma} c_{r\mathbf{k}\sigma}^\dagger c_{r\mathbf{k}\sigma}$ for the left ($r = L$) and right ($r = R$) lead, where $\varepsilon_{r\mathbf{k}\sigma}$ is the energy of an electron with the wave vector \mathbf{k} and spin σ in the lead r , and $c_{r\mathbf{k}\sigma}^\dagger$ ($c_{r\mathbf{k}\sigma}$) denotes the respective creation (annihilation) operator. The double dot is described by the Hamiltonian

$$H_{\text{DQD}} = \sum_{j=1,2} \sum_{\sigma} \varepsilon_j n_{j\sigma} + U \sum_{j=1,2} n_{j\uparrow} n_{j\downarrow} + U' \sum_{\sigma\sigma'} n_{1\sigma} n_{2\sigma'} + t \sum_{\sigma} (d_{1\sigma}^\dagger d_{2\sigma} + d_{2\sigma}^\dagger d_{1\sigma}), \quad (2)$$

with $n_{j\sigma} = d_{j\sigma}^\dagger d_{j\sigma}$, where $d_{j\sigma}^\dagger$ ($d_{j\sigma}$) is the creation (annihilation) operator of an electron with spin σ in the first ($j = 1$) or second ($j = 2$) quantum dot, and ε_j is the corresponding single-particle energy. The Coulomb interaction on the first and second dot is assumed to be equal and is described by U , while U' corresponds to the inter-dot Coulomb correlation. The last term of H_{DQD} describes the hopping between the two dots with t being the hopping parameter. We assume that the hopping parameter is large, so that there is a considerable overlap of the wave functions of the two dots, leading to the formation of molecular many-body states, through which transport takes place. In addition, we also note that an exchange interaction between spins in the two dots may lead to the formation of singlet and triplet states.¹² However, experimentally, this exchange interaction was found to be rather small as compared to the other energy scales,⁶ therefore, in the following considerations, we will neglect it.

The tunneling processes between the DQD and elec-

trodes are described by the Hamiltonian,

$$H_T = \sum_{r=L,R} \sum_{j=1,2} \sum_{\mathbf{k}\sigma} \left(t_{rj} c_{r\mathbf{k}\sigma}^\dagger d_{j\sigma} + t_{rj}^* d_{j\sigma}^\dagger c_{r\mathbf{k}\sigma} \right), \quad (3)$$

where t_{rj} denotes the tunnel matrix elements between the r th lead and the j th dot. The coupling of the j th dot to the r th lead can be written as $\Gamma_{rj}^\sigma = 2\pi |t_{rj}|^2 \rho_r^\sigma$, where ρ_r^σ is the spin-dependent density of states of lead r . By introducing the definition of the spin polarization of lead r , $p_r = (\rho_r^+ - \rho_r^-)/(\rho_r^+ + \rho_r^-)$, one can write, $\Gamma_{rj}^{+(-)} = \Gamma_{rj}(1 \pm p_r)$, with $\Gamma_{rj} = (\Gamma_{rj}^+ + \Gamma_{rj}^-)/2$, where Γ_{rj}^+ and Γ_{rj}^- describe the coupling of the j th dot to the spin-majority and spin-minority electron bands of the lead r , respectively.

Because the double dot Hamiltonian, Eq. (2), is not diagonal in the local basis, we perform a unitary transformation, $U^\dagger H_{\text{DQD}} U = \tilde{H}_{\text{DQD}}$, to a new basis in which \tilde{H}_{DQD} is diagonal, $\tilde{H}_{\text{DQD}}|\chi\rangle = \varepsilon_\chi|\chi\rangle$. The eigenvectors $|\chi\rangle$ are the many-body states of the double quantum dot, while the eigenvalues ε_χ denote the corresponding energies.⁷⁴

III. METHOD

In order to calculate the spin-dependent transport properties of a double quantum dot in the sequential and cotunneling regimes, we employ the real-time diagrammatic technique.^{43,75,76} It consists in a systematic perturbation expansion of the reduced density matrix of the considered system and the current operator with respect to the dot-lead coupling strength Γ . The time evolution of the reduced density matrix can be visualized as a sequence of irreducible self-energy blocks, $W_{\chi\chi'}$, on the Keldysh contour, where $W_{\chi\chi'}$ describe transitions between the many-body DQD states $|\chi\rangle$ and $|\chi'\rangle$. The elements $W_{\chi\chi'}$ set up a self-energy matrix \mathbf{W} . Within the matrix notation introduced by Thielmann *et al.*,⁷⁶ the stationary elements of the reduced density matrix can be found from

$$(\tilde{\mathbf{W}}\mathbf{p}^{\text{st}})_\chi = \Gamma\delta_{\chi\chi_0}, \quad (4)$$

where \mathbf{p}^{st} is the vector containing probabilities and the matrix $\tilde{\mathbf{W}}$ is the modified matrix \mathbf{W} so as to include the normalization of probabilities. The current flowing through the system can be then found from

$$I = \frac{e}{2\hbar} \text{Tr}\{\mathbf{W}^I \mathbf{p}^{\text{st}}\}. \quad (5)$$

The matrix \mathbf{W}^I is the self-energy matrix with one *internal* vertex resulting from the expansion of the tunneling Hamiltonian replaced by the current operator.

To calculate the transport properties order by order in tunneling processes, we expand the self-energy matrices, $\mathbf{W} = \mathbf{W}^{(1)} + \mathbf{W}^{(2)} + \dots$, $\mathbf{W}^I = \mathbf{W}^{I(1)} + \mathbf{W}^{I(2)} + \dots$, and

the dot occupations, $\mathbf{p}^{\text{st}} = \mathbf{p}^{\text{st}(0)} + \mathbf{p}^{\text{st}(1)} + \dots$, respectively. Then, the first-order (sequential) and the second-order (cotunneling) currents are given by

$$\begin{aligned} I^{(1)} &= \frac{e}{2\hbar} \text{Tr}\{\mathbf{W}^{I(1)} \mathbf{p}^{\text{st}(0)}\}, \\ I^{(2)} &= \frac{e}{2\hbar} \text{Tr}\{\mathbf{W}^{I(2)} \mathbf{p}^{\text{st}(0)} + \mathbf{W}^{I(1)} \mathbf{p}^{\text{st}(1)}\}. \end{aligned} \quad (6)$$

On the other hand, the zeroth and first-order occupation probabilities can be found from the following equations

$$\begin{aligned} (\tilde{\mathbf{W}}^{(1)} \mathbf{p}^{\text{st}(0)})_\chi &= \Gamma\delta_{\chi\chi_0}, \\ \tilde{\mathbf{W}}^{(1)} \mathbf{p}^{\text{st}(1)} + \tilde{\mathbf{W}}^{(2)} \mathbf{p}^{\text{st}(0)} &= 0, \end{aligned} \quad (7)$$

where $\tilde{\mathbf{W}}^{(1)} [\tilde{\mathbf{W}}^{(2)}]$ is given by $\mathbf{W}^{(1)} [\mathbf{W}^{(2)}]$ with one arbitrary row χ_0 replaced by (Γ, \dots, Γ) $[(0, \dots, 0)]$ due to the normalization of probabilities, $\sum_\chi p_\chi^{\text{st}(n)} = \delta_{n,0}$.

As one can see from the above formulas, to determine the transport properties it is necessary to calculate the elements of the corresponding self-energy matrices. This can be done using the respective diagrammatic rules.^{43,75,76} Although the first-order calculation is rather simple, the general analytical formulas for the self-energies in the second order are rather complicated due to many virtual states through which the cotunneling processes can take place. In the Appendix A, as an example, we present the contribution coming from $W_{\chi(N),\chi'(N)}^{(2)}$ where N is the charge state of the double dot.

In addition, in the present paper we also analyze the zero-frequency current noise of the double quantum dot system, $S = 2 \int_{-\infty}^0 dt (\langle \hat{I}(t) \hat{I}(0) + \hat{I}(0) \hat{I}(t) \rangle - 2\langle \hat{I} \rangle^2)$. For low bias voltages the current noise is dominated by thermal noise, while for $|eV| > k_B T$ the noise associated with the discrete nature of charge (shot noise) dominates.⁸⁰ Within the real-time diagrammatic technique, a general formula for the shot noise has been derived in Ref. [76] taking into account the non-Markovian effects. The shot noise in the first-order can be found from the corresponding expression

$$S^{(1)} = \frac{e^2}{\hbar} \text{Tr} \left[\left(\mathbf{W}^{II(1)} + \mathbf{W}^{I(1)} \mathbf{P}^{(-1)} \mathbf{W}^{I(1)} \right) \mathbf{p}^{\text{st}(0)} \right], \quad (8)$$

while the cotunneling current noise is given by

$$\begin{aligned} S^{(2)} &= \frac{e^2}{\hbar} \text{Tr} \left\{ \left[\mathbf{W}^{II(2)} + \mathbf{W}^{I(2)} \mathbf{P}^{(-1)} \mathbf{W}^{I(1)} \right. \right. \\ &\quad + \mathbf{W}^{I(1)} \mathbf{P}^{(-1)} \mathbf{W}^{I(2)} + \mathbf{W}^{I(1)} \mathbf{P}^{(0)} \mathbf{W}^{I(1)} \\ &\quad + \left. \left. \mathbf{W}^{I(1)} \mathbf{Q}^{(0)} \partial \mathbf{W}^{I(1)} \right] \mathbf{p}^{\text{st}(0)} \right. \\ &\quad \left. + \left[\mathbf{W}^{II(1)} + \mathbf{W}^{I(1)} \mathbf{P}^{(-1)} \mathbf{W}^{I(1)} \right] \mathbf{p}^{\text{st}(1)} \right\}, \end{aligned} \quad (9)$$

where $\mathbf{Q}^{(n)} = \mathbf{p}^{\text{st}(n)} \otimes \mathbf{e}^T$, with $\mathbf{e}^T = (1, \dots, 1)$. The objects $\mathbf{P}^{(-1)}$ and $\mathbf{P}^{(0)}$ are given by, $\tilde{\mathbf{W}}^{(1)} \mathbf{P}^{(-1)} = \mathbf{Q}^{(1)} - \mathbf{1}$, and, $\tilde{\mathbf{W}}^{(1)} \mathbf{P}^{(0)} + \tilde{\mathbf{W}}^{(2)} \mathbf{P}^{(-1)} = \tilde{\mathbf{1}}(\mathbf{Q}^{(1)} - \partial \mathbf{W}^{(1)} \mathbf{Q}^{(0)})$, respectively, with $\tilde{\mathbf{1}}$ being the unit vector with row χ_0 set to zero. On the other hand, the matrices $\mathbf{W}^{II(1)}$ and $\mathbf{W}^{II(2)}$

are the first and second-order self-energy matrices with two internal vertices replaced by the current operator, while $\partial \mathbf{W}^{(1)}$ and $\partial \mathbf{W}^{I(1)}$ are partial derivatives of $\mathbf{W}^{(1)}$ and $\mathbf{W}^{I(1)}$ with respect to the convergence factor of the Laplace transform.⁷⁶

By taking into account all the first-order and second-order contributions to the self-energies, we are able to resolve the transport properties in the full range of the bias and gate voltages. The first order of expansion with respect to the coupling corresponds to sequential tunneling, while the second order is associated with cotunneling. Sequential tunneling is allowed if the applied bias is larger than the threshold voltage, i.e. when the energy provided by the transport voltage is comparable with the charging energy. Otherwise, the system is in the Coulomb blockade regime where sequential tunneling is exponentially suppressed and the current flows due to cotunneling, which involves correlated tunneling through virtual states of the system.^{77,78,79}

Among different cotunneling processes one can generally distinguish two types of processes: non-spin-flip ones, which do not affect the DQD state, and the spin-flip ones. Furthermore, one can also have double-barrier cotunneling, which contributes directly to the current, and single-barrier cotunneling, which affects the double dot occupations and, thus, indirectly, the current.

IV. DOUBLE QUANTUM DOTS COUPLED IN SERIES

In this section we present and discuss numerical results on double quantum dots coupled in series. In order to realize this geometry we set $\Gamma_{L2} = \Gamma_{R1} = 0$ and assume $\Gamma_{L1} = \Gamma_{R2} \equiv \Gamma/2$, see Fig. 1. Furthermore, in the following we will also distinguish between symmetric and asymmetric DQDs. In the former case, the level position of each dot is the same, $\varepsilon_1 = \varepsilon_2$, while in the latter case the levels are detuned, $\varepsilon_1 \neq \varepsilon_2$. In addition, in this section we will emphasize the role of second-order processes in transport. In order to ascribe observed features to respective tunneling processes, we will therefore also present results obtained within the sequential tunneling approximation, i.e. when considering only the first-order tunneling processes.

A. Symmetric double quantum dots

The differential conductance as a function of the bias voltage and the position of the dot levels for the parallel and antiparallel configurations is shown in Fig. 2(a) and (b). Because experimentally the position of the dots' levels can be changed upon applying a gate voltage, Fig. 2 effectively shows the bias and gate voltage dependence of the conductance. First of all, it can be seen that the differential conductance displays a characteristic Coulomb diamond structure. The diamonds in the low bias volt-

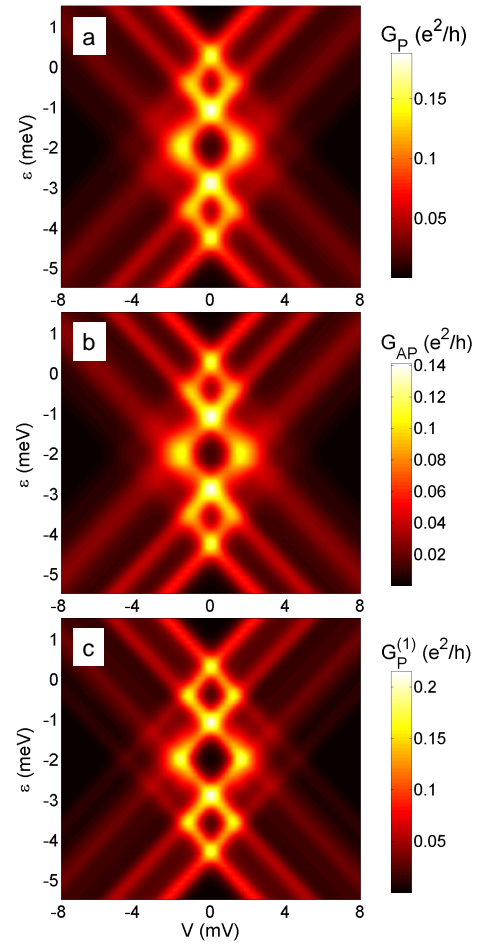


FIG. 2: (Color online) The differential conductance in the parallel G_P (a) and antiparallel G_{AP} (b) magnetic configurations as a function of the bias voltage V and the position of the dots' levels $\varepsilon \equiv \varepsilon_1 = \varepsilon_2$ for double quantum dots coupled in series. The parameters are: $k_B T = 0.15$ meV, $U = 2$ meV, $U' = 1$ meV, $t = 0.25$ meV, $\Gamma_{L2} = \Gamma_{R1} = 0$, $\Gamma_{L1} = \Gamma_{R2} \equiv \Gamma/2$, with $\Gamma = 0.1$ meV, and $p = 0.5$. Because the double quantum dot is symmetric, $\varepsilon_1 = \varepsilon_2$, there is no asymmetry associated with the bias reversal. For comparison in part (c) we also show the density plot of the differential conductance in the parallel configuration calculated using only the first-order tunneling processes, $G_P^{(1)}$.

age regime correspond to the Coulomb blockade regime where the sequential current is exponentially suppressed and the current flows due to cotunneling. With increasing the bias voltage the excited states start participating in transport, which leads to additional lines in the differential conductance. The features described above are rather associated with the energy spectrum and charge states of the DQD than with the ferromagnetism of the leads, therefore they are present in both magnetic configurations. The spin dependence stemming from ferromagnetic electrodes gives rise to a difference of the conductance in the parallel and antiparallel configurations, see Fig. 2(a) and (b). The conductance in the parallel

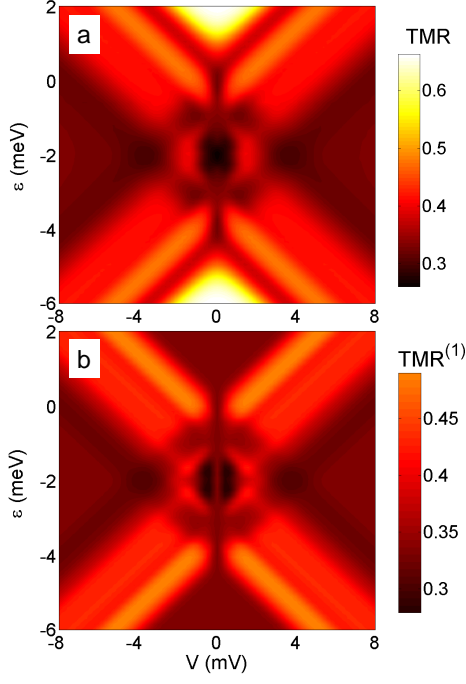


FIG. 3: (Color online) The total (first and second order) TMR (a) and the first-order TMR (b) as a function of the bias voltage V and the level position ε for parameters the same as in Fig. 2. The two figures are plotted in the same scale.

configuration is generally larger than that in the antiparallel configuration. This is due to the spin asymmetry in the couplings when the leads' magnetizations are antiparallel. As in the parallel configuration the majority (minority) electrons of, let us say, left lead tunnel to the majority (minority) electron band of the right lead, in the antiparallel configuration the situation is reversed – the majority (minority) electrons of the left lead tunnel to the minority (majority) electron band of the right lead. This leads to the difference of the conductance in both magnetic configurations, see Fig. 2, and to the corresponding tunnel magnetoresistance effect. In addition, in Fig. 2(c) we also present the bias and gate voltage dependence of the differential conductance for the parallel configuration calculated within the sequential tunneling approximation, $G_P^{(1)}$. By comparing Fig. 2(a) and (c), one can see that cotunneling leads to broadening of the resonance peaks, lowering the magnitude of the differential conductance, and gives rise to finite conductance in the Coulomb blockade regimes.

The bias and gate voltage dependence of the TMR is shown in Fig. 3(a), while Fig. 3(b) presents the first-order TMR, $\text{TMR}^{(1)}$. Intuitively, the TMR is a measure of the system's transport properties change when the magnetic configuration switches from the parallel to the antiparallel one. It is defined as^{37,38,43}

$$\text{TMR} = \frac{I_P - I_{AP}}{I_{AP}}, \quad (10)$$

where I_P (I_{AP}) is the current flowing through the sys-

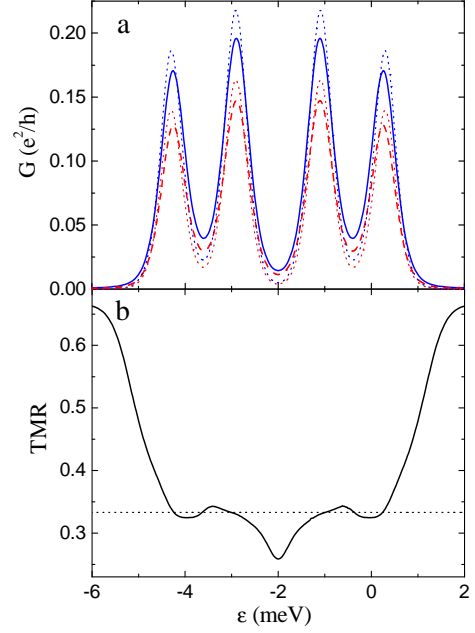


FIG. 4: (Color online) The linear conductance in the parallel (solid line) and antiparallel (dashed line) magnetic configurations (a) and the linear TMR (b) as a function of the level position ε for parameters the same as in Fig. 2. For comparison, the dotted curves show the linear conductance and the TMR calculated taking into account only the first-order processes.

tem in the parallel (antiparallel) configuration. By comparison with Fig. 2, one can easily identify the different transport regimes. Furthermore, by comparing the total and sequential TMR, one can immediately see that cotunneling modifies the TMR mainly in the low bias voltage regime, i.e. in the Coulomb blockade regime and in the regime where sequential tunneling is suppressed due to the absence of levels in the energy window provided by transport voltage. In order to discuss and see more clearly the behavior of the TMR on applied voltages, in Fig. 4 we show the linear response conductance and resulting TMR, while in Fig. 5 we display the transport properties in the nonlinear response regime.

The linear conductance in both magnetic configurations is shown in Fig. 4(a). When lowering the position of the DQD levels the conductance displays four resonance peaks associated with subsequent occupation of the corresponding charge states. The dotted curves in Fig. 4 present results obtained in the first-order approximation. It can be seen that off resonance the current is mainly dominated by cotunneling. On the other hand, on resonance the sequential processes dominate current, while cotunneling only slightly affects the conductance, leading to renormalization of the DQD levels and, thus, slightly shifting the position of the conductance peaks, see Fig. 4(a). Interestingly, the second-order processes have a rather large impact on the linear TMR shown in Fig. 4(b). First of all, the linear response TMR exhibits

a strong dependence on the gate voltage, i.e. on the number of electrons in the double quantum dot. When the DQD is either empty or fully occupied, the TMR is given by the Julliere value, $\text{TMR} = 2p^2/(1 - p^2)$.³⁷ This is due to the fact that in those transport regimes the current is driven by elastic cotunneling processes which do not affect the DQD state in any way. Thus, as far as the TMR is concerned, the system behaves as a single ferromagnetic tunnel junction.³⁷ However, in the Coulomb blockade regions, the TMR becomes generally suppressed due to the presence of inelastic cotunneling which introduces spin-flip processes in the system. The dotted line in Fig. 4(b) shows the TMR calculated within the sequential tunneling approximation – it is given by $\text{TMR} = p^2/(1 - p^2)$.^{43,55} At this point, we would like to note that the results for the linear conductance calculated by including only the first-order processes are rather reliable in the whole range of ε . On the other hand, the results for the linear response TMR are comparable to those obtained within the sequential tunneling approximation only on resonance, where sequential processes dominate, while off resonance they are completely unreliable, see Fig. 4. Therefore, in order to properly analyze the dependence of the TMR in the full range of parameters one has to take into account cotunneling processes.

The bias voltage dependence of the current, differential conductance, tunnel magnetoresistance and the Fano factor is shown in Fig. 5 for $\varepsilon = -2$ meV and $\varepsilon = 2$ meV. The first situation, $\varepsilon = -2$ meV, corresponds to the case when the ground state of the double quantum dot is doubly occupied, while the second one, $\varepsilon = 2$ meV, corresponds to the case of empty double dot. In all cases, due to the spin asymmetry of tunneling processes, the current in the parallel configuration is larger than the current in the antiparallel configuration. In addition, the i - v curves display characteristic Coulomb steps. With increasing the bias voltage more and more charge states start to participate in transport which gives rise to the corresponding steps in the current-voltage characteristics, and peaks in the differential conductance. Furthermore, the single-electron charging effects also lead to the oscillatory-like behavior of the TMR effect, see Fig. 5(c) and (g). In the Coulomb blockade regime, $\varepsilon = -2$ meV, the TMR is much suppressed as compared to the case of $\varepsilon = 2$ meV. This is due to the presence of spin-flip cotunneling processes in the case of the doubly occupied DQD, as already discussed in association with Fig. 4. However, when increasing the bias voltage the TMR increases and, at the threshold for sequential tunneling, reaches a local maximum, see Fig. 5(c). This effect is due to the nonequilibrium spin accumulation which is induced in the DQD system with increasing the transport voltage. (Similar effect can be observed when the double dot is singly occupied, i.e. when $\varepsilon = -0.5$ meV.) On the other hand, when the DQD is empty, the TMR at low bias voltage acquires the Julliere value,³⁷ and then, with increasing V , becomes generally suppressed, see Fig. 5(g).

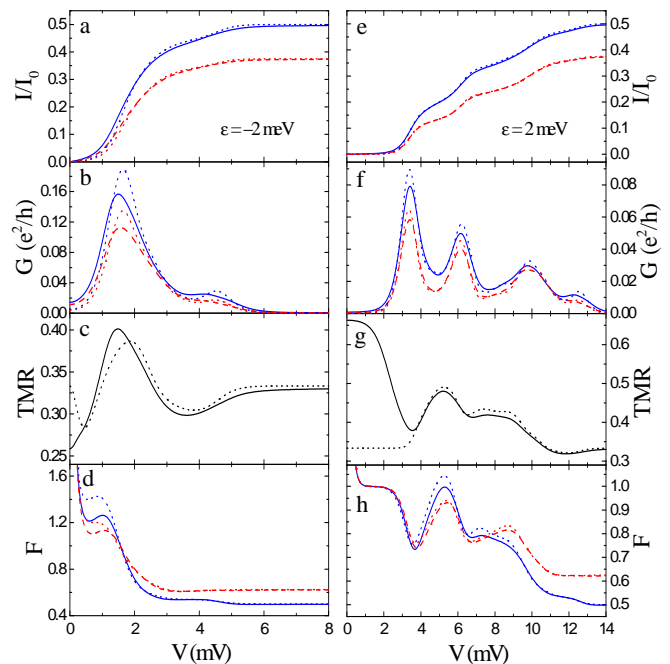


FIG. 5: (Color online) The current in units of $I_0 = e\Gamma/\hbar$ (a,e), differential conductance (b,f) and the Fano factor (d,h) in the parallel (solid line) and antiparallel configuration (dashed line) as well as the TMR (c,g) as a function of the bias voltage for different values of the level position ε as indicated in the figure. $\varepsilon = -2$ meV (a-d) corresponds to the case when the ground state of the DQD is doubly occupied, while for $\varepsilon = 2$ meV (e-h) the double dot is empty. The parameters are the same as in Fig. 2. The dotted curves show the results obtained in the sequential tunneling approximation.

In addition, in Fig. 5 we also show the Fano factor, $F = S/(2e|I|)$, calculated in both magnetic configurations and for two values of ε , as indicated in the figure. First of all, one can see that the Fano factor becomes divergent at low bias voltages. This is due to the thermal noise which dominates the current noise as $V \rightarrow 0$, while $I \rightarrow 0$, leading to $F \rightarrow \infty$.⁸⁰ Furthermore, it can be seen that the Fano factor in the Coulomb blockade regime is slightly larger in the parallel configuration than in the antiparallel one. This is associated with an additional positive cross-correlations, which contribute to the current noise, due to the ferromagnetism of the electrodes. In the Coulomb blockade regime, there is a larger asymmetry between the cotunneling processes through the majority and minority spin channels in the parallel configuration than in the antiparallel one. This effectively increases the current fluctuations in the parallel configuration and leads to the corresponding difference in the Fano factors, see Fig. 5(d). On the other hand, in the sequential tunneling regime, the information about the spin asymmetry of tunneling processes between the DQD and the corresponding lead is rather contained in the nonequilibrium spin accumulation induced in the double dot. This spin accumulation is larger in the an-

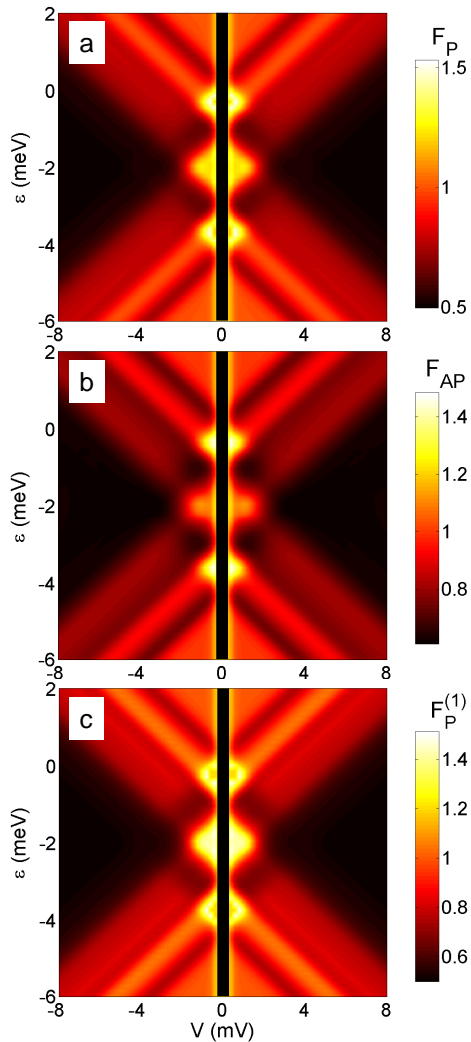


FIG. 6: (Color online) The total Fano factor in the parallel (a) and antiparallel (b) magnetic configurations as a function of the bias voltage V and the position of the dots' levels ε for parameters the same as in Fig. 2. Part (c) presents the Fano factor in the parallel configuration calculated in the first-order approximation. Because the Fano factor is divergent for $|eV| \lesssim k_B T$, this transport regime is denoted with a thick black line.

tiparallel configuration, yielding generally an enhanced Fano factor in the antiparallel configuration as compared to the parallel one. Moreover, we also note that in the Coulomb blockade regime, $\varepsilon = -2$ meV, the shot noise becomes super-Poissonian ($F > 1$) and drops to the sub-Poissonian value ($F < 1$) at the threshold for sequential tunneling, see Fig. 5(d). This super-Poissonian shot noise is associated with bunching of inelastic cotunneling processes through the system.^{54,81} On the other hand, in the case of empty DQD, $\varepsilon = 2$ meV, in the cotunneling regime the current flows due to elastic second-order processes which obey the Poissonian statistics. In this case the shot noise is given by $S = 2e|I|$ and the Fano factor is simply equal to unity, see Fig. 5(h), irrespective

of magnetic configuration of the system. As concerns the sequential tunneling regime, the shot noise is then generally sub-Poissonian, irrespective of the position of the DQD level ε . This indicates the role of correlations in electronic transport, in particular, the Coulomb correlations and charge conservation.⁸⁰ Our results are in qualitative agreement with experimental data on tunneling through vertically coupled self-assembled InAs quantum dots where also super-Poissonian shot noise has been found.¹⁹

Finally, to make the present analysis self-contained, we also show the bias and gate voltage dependence of the total Fano factor for the parallel and antiparallel magnetic configuration, see Fig. 6(a) and (b), respectively. In addition, for comparison, the Fano factor calculated by taking into account only first-order tunneling processes is depicted in Fig. 6(c). The black lines around the zero bias, $|eV| \lesssim k_B T$, mark the transport regime where the Fano factor is divergent due to finite thermal noise. The different behavior of the shot noise is now clearly visible. In the Coulomb blockade regime the noise is super-Poissonian, in the cotunneling regime when the DQD is either empty or fully occupied (current is mediated by elastic cotunneling) the shot noise is Poissonian, and in the sequential tunneling regime the noise drops to sub-Poissonian value.

B. Asymmetric double quantum dots: Pauli spin blockade

By applying a gate voltage to each quantum dot, it is possible to tune the dot levels separately. So far, we have considered the case of symmetric DQD, i.e. when $\varepsilon_1 = \varepsilon_2$. In this situation the transport characteristics were symmetric with respect to the bias reversal. This is however not the case for $\varepsilon_1 \neq \varepsilon_2$, where the current becomes asymmetric with respect to the bias reversal, leading to the Pauli spin blockade and negative differential conductance, as observed experimentally.^{6,8} In the following, assuming realistic parameters of the double quantum dot system, we analyze transport properties in the regime where the Pauli spin blockade effects are visible.

The mechanism leading to the spin blockade was theoretically discussed by Fransson *et al.*¹⁵ and Muralidharan *et al.*¹⁸ These considerations were however restricted only to the first-order tunneling processes, which dominate the current out of the blockade regime. As shown experimentally by Ono *et al.*,⁶ in the spin blockade regime there is a finite leakage current, which cannot be explained within the sequential tunneling approximation. To explain the existence of this leakage, it was proposed that non-zero current in the Pauli blockade is associated with spin-flip processes induced by hyperfine interaction.¹⁷ In the following, we show that the leakage current results just from the interplay between different intrinsic tunneling processes driving the current. The hyperfine interaction, or coupling to a phonon bath, may, of course, increase the

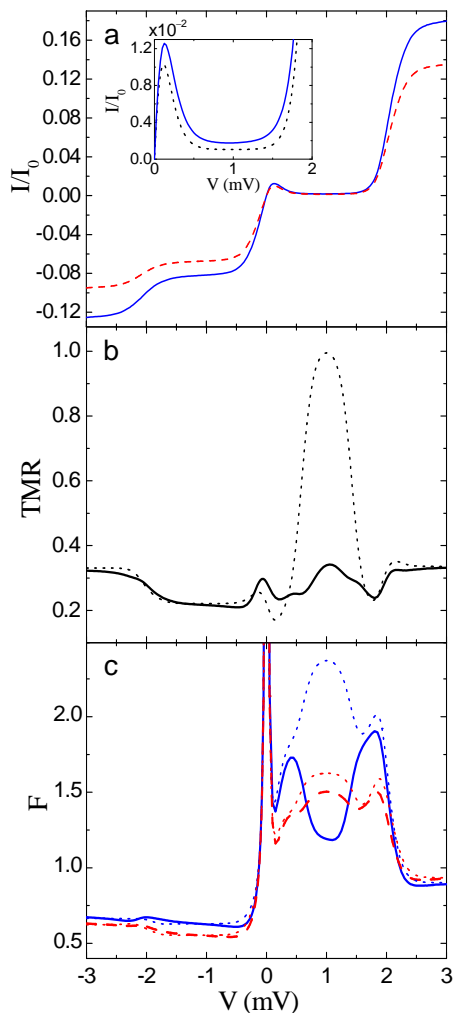


FIG. 7: (Color online) The current (a) and Fano factor (c) in the parallel (solid) and antiparallel (dashed) magnetic configurations as well as the TMR (b) as a function of the bias voltage for DQD coupled in series. The parameters are: $k_B T = 0.05$ meV, $\varepsilon_1 = -1$ meV, $\varepsilon_2 = -2$ meV, $\Delta = 3$ meV, $U = 2$ meV, $U' = 1$ meV, $t = 0.05$ meV, where Δ is the level spacing in each dot. The other parameters are the same as in Fig. 2. The inset in part (a) displays the current in the parallel magnetic configuration in the Pauli spin blockade regime. The dotted lines correspond to the first-order calculation.

leakage, but is not necessary for the observation of a finite current in the Pauli spin blockade regime.

When the DQDs levels are detuned, $\varepsilon_2 < \varepsilon_1$, and once the first and second dot become singly occupied, the current may be suppressed in some range of the bias voltage. This is associated with the full occupation of two-electron triplet states of the DQD.¹⁵ The Pauli spin blockade may be lifted when the applied bias voltage admits another (excited) charge states to participate in transport. On the other hand, when the voltage is reversed, it is energetically allowed that the electron from the first dot tunnels to the left lead and then another electron from the right lead enters the DQD, lifting the Pauli spin blockade.

This can be seen in Fig. 7 where we present the bias voltage dependence of the current, Fano factor and the TMR effect. In order to make the calculations more realistic and to allow for excited states of the system, we have now taken into account four different orbital levels, two in each dot. Such system is described by straightforward extension of the hamiltonian, Eq. (2), where the level spacing in the dots is described by the parameter Δ . First of all, one can see that the transport characteristics are asymmetric with respect to the bias reversal. This is associated with the fact that by detuning the DQDs levels the symmetry of transition rates between the left and right leads has been broken. Furthermore, for positive bias voltage the current is suppressed in a broad range of the bias voltage ($0 < eV < U$) due to the full occupation of the triplet states, while for negative bias the Pauli spin blockade is lifted. In addition, the blockade can also be lifted when the positive bias voltage is increased further, $eV > U$, so that tunneling through the second level of the second dot is allowed, see Fig. 7(a).

In the inset of Fig. 7(a) we show the current in the parallel configuration just in the spin blockade regime. For comparison, we also display the current calculated within the sequential tunneling approximation. One can see that the sequential current is suppressed as compared to the total current (calculated taking into account cotunneling processes). The suppression of the sequential current is generally governed by the ratio $2t/|\varepsilon_2 - \varepsilon_1|$.¹⁵ When $2t/|\varepsilon_2 - \varepsilon_1| \ll 1$, the occupation of the two-electron triplet states approaches unity and the first-order current becomes fully blocked. However, the second-order processes are still allowed, leading to a finite leakage current in the spin blockade regime. One can distinguish different contributions coming from cotunneling:

- (i) The double-barrier elastic second-order processes which contribute directly to the current.
- (ii) The double-barrier spin-flip cotunneling which contributes to the current and reduces the occupation of the triplet state, this way opening the DQD for the sequential tunneling.
- (iii) The single-barrier spin-flip cotunneling which does not contribute directly to the current but flips the spin in the DQD and allows the sequential processes to occur.

As a consequence, in the Pauli spin blockade regime the current flows due to cotunneling and spin-flip cotunneling-assisted sequential tunneling. The key role is played by the spin-flip processes which decrease the occupation of the two-electron triplet states and lead to a finite occupation of singlet states. The importance of the spin-flip processes in explanation of the finite leakage current has been invoked in Ref. [17]. The leakage was there associated with spin-flip processes induced by hyperfine interaction through the Overhauser effect. Here, we show that the leakage results just from the interplay between different tunneling processes, i.e. just from the pure nature of tunneling processes. We also note that the effects of cotunneling are rather independent of the material from which the dots are built, unlike the Overhauser

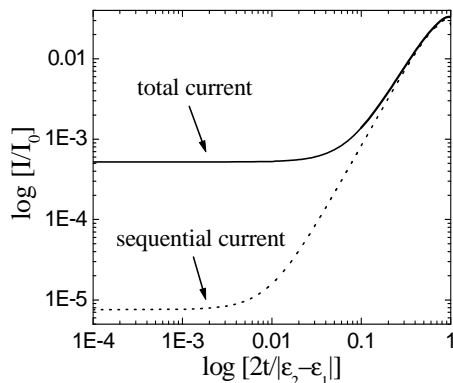


FIG. 8: The total (sequential plus cotunneling) current (solid line) and the sequential current (dotted line) in the parallel configuration as a function of the hopping between the two dots calculated in the middle of the Pauli spin blockade regime, $V = 1$ mV. The parameters are the same as in Fig. 7. The dependence of the current on $2t/|\varepsilon_2 - \varepsilon_1|$ in the antiparallel configuration is qualitatively similar.

field.⁸² Thus, for example, in GaAs DQDs the leakage current in the Pauli spin blockade would be associated with both cotunneling and hyperfine contributions, while in carbon nanotube DQDs it would be mainly due to cotunneling. Furthermore, as shown in experiments by Ono and Tarucha,⁸³ who studied the dependence of the leakage current on the applied magnetic field, the hyperfine interaction starts to play a role at certain finite in-plane magnetic fields, at which the nuclei become polarized, leading to a sudden jump of the leakage current as a function of magnetic field. This suggests that the main contribution to the current in the spin blockade regime in the absence of magnetic field may come from cotunneling. In the weak coupling regime, typical values of the dot-lead coupling strength Γ are of the order of μeV ,⁸⁴ which gives the leakage current of the order of $10^{-3}I_0 \approx 1$ pA (see Fig. 8), in agreement with experimental results.⁸³ Finally, we notice that to explain the jump in the leakage current when sweeping magnetic field, besides cotunneling, one also has to include the hyperfine interaction. Nevertheless, this goes beyond the scope of the present paper.

In Fig. 8 we present the logarithmic dependence of the sequential and total currents in the parallel configuration on the hopping parameter t . It is clearly visible that for $2t/|\varepsilon_2 - \varepsilon_1| \ll 1$, the sequential current is smaller by two orders of magnitude than the total current. On the other hand, when $2t/|\varepsilon_2 - \varepsilon_1| \approx 1$, the sequential current becomes of the same order as the total current, but still, noticeably, the total current is larger than that calculated using only the first-order tunneling processes. The saturation of the two currents for $2t/|\varepsilon_2 - \varepsilon_1| \ll 1$, see Fig. 8, is associated with a finite temperature. However, because sequential tunneling depends exponentially on temperature while cotunneling only algebraically, at lower T the difference between the two currents would be

even more pronounced. The dependence of the current in the antiparallel configuration is qualitatively similar to the one shown in Fig. 8. We also note that generally the above mentioned mechanism responsible for the leakage current does not depend on whether the leads are made of ferromagnetic or nonmagnetic material.

The TMR as a function of the bias voltage is displayed in Fig. 7(b). One can see that the TMR calculated using the first-order processes and that calculated taking into account cotunneling are generally similar, except for the Pauli spin blockade regime. In this transport regime the sequential TMR is much overestimated. To understand this behavior we note again that the blockade results from the full occupation of DQD's triplet states. The probability is equally distributed between the three components of the triplet in the parallel configuration. However, in the antiparallel configuration, it turns out that the charge is mainly accumulated in the $S_z = 1$ component of the triplet. As a consequence, in the parallel configuration all the three components of the triplet participate in transport, while in the antiparallel configuration only one. Because the sequential current in the blockade regime is mainly associated with thermal fluctuations, the difference in the number of states relevant for transport leads to large sequential TMR in blockade regime. This difference also gives rise to the corresponding difference between Fano factors calculated in the sequential tunneling approximation, see the dotted curves in Fig. 7(c). The shot noise is then super-Poissonian and larger in the parallel configuration. However, as pointed above, the leakage current in the Pauli spin blockade regime is due to cotunneling and cotunneling-assisted sequential tunneling processes. The total current flows not only due to thermal fluctuations but due to correlated tunneling through virtual states of the DQD. This fact generally decreases the current fluctuations and the difference between the two magnetic configurations. As a result, the total TMR and Fano factor become suppressed as compared to the sequential tunneling results, see Fig. 7(b) and (c), respectively. In addition, we also notice that, irrespective of the magnetic configuration of the system, the shot noise is super-Poissonian in the spin blockade regime and drops to sub-Poissonian value out of the blockade regime, see Fig. 7(c). The super-Poissonian shot noise is generally due to bunching of spin-flip cotunneling and cotunneling-assisted sequential tunneling processes.

V. DOUBLE QUANTUM DOTS COUPLED IN PARALLEL

In this section we analyze the spin-polarized transport through double quantum dots coupled in parallel. This geometry can be realized by setting $\Gamma_{rj} \equiv \Gamma/2$, for $r = L, R$ and $j = 1, 2$, see Fig. 1. We note that in the case of negligible hopping between the two quantum dots, $t \rightarrow 0$, the behavior of the DQD system resembles that of a

single multi-level quantum dot. The problem of spin-dependent transport through multi-level quantum dots has been addressed very recently in Ref. [54] and will not be considered here.

In Fig. 9 we present the density plots of the differential conductance and Fano factor in the parallel configuration as well as of the TMR effect as a function of the bias and gate voltages. The behavior of the conductance and the shot noise in the antiparallel configuration is qualitatively similar as in the parallel configuration, therefore, it is not shown here. The information about the difference in transport in the two magnetic alignments is contained in the TMR, whose magnitude reflects the asymmetry in tunneling processes when the leads are parallel or antiparallel to each other.

The differential conductance, shown in Fig. 9(a), displays characteristic Coulomb diamonds. Because the internal energy structure of the DQD is generally the same as in the case of DQD coupled in series, the differential conductances are qualitatively similar, see Figs. 2(a) and 9(a). The main difference is that in the case of parallel DQDs the level of each dot is coupled both to the left and right leads, which generally results in an enhanced conductance for parallel DQDs as compared to DQDs coupled in series. Similarly the TMR shown in Fig. 9(b), its bias and gate voltage dependence is only slightly modified as compared to Fig. 3(a). Again, the linear TMR exhibits a strong dependence on the occupation number of the DQD, with TMR given by the Julliere formula for empty and fully occupied double quantum dot, and is much suppressed in other transport regimes due to spin-flip cotunneling. In the Coulomb blockade regime, the transport properties are mainly conditioned by the spin-flip cotunneling, which gives a dominant contribution to the current. Furthermore, the bunching of spin-flip cotunneling in the Coulomb blockade regime leads to super-Poissonian shot noise, see Fig. 9(c). The super-Poissonian shot noise is however more pronounced in Coulomb blockade regimes with an odd number of electrons in the double dot. On the other hand, for voltages above the threshold for sequential tunneling, the shot noise becomes sub-Poissonian, with the Fano factor approaching $1/2$.

Summing up, we notice that generally in the weak coupling regime the effect of different geometries of the double dot system leads only to qualitative difference in transport properties. The main difference is in the magnitude of conductance – for parallel DQDs it is roughly two times larger than for serial DQDs. This is contrary to the strong coupling regime where, for example, in the parallel geometry the orbital Kondo phenomenon arises due to the interference effects, while for DQDs coupled in series the orbital Kondo effect is destroyed.⁸⁵ Finally, we also note that in the case of detuned levels, $|\varepsilon_2 - \varepsilon_1| \gg 0$, transport properties of double quantum dots coupled in parallel are qualitatively similar to those of single multi-level quantum dots.⁵⁴

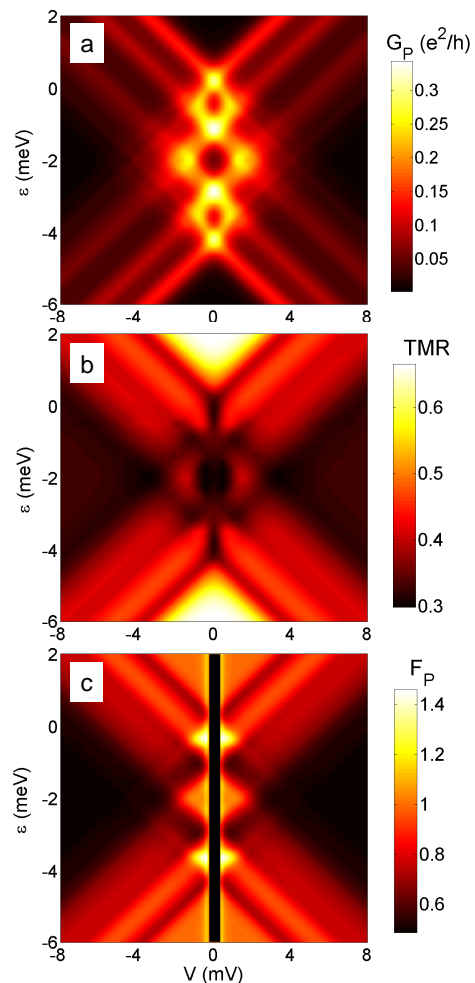


FIG. 9: (Color online) The differential conductance (a) and Fano factor (c) in the parallel magnetic configuration, and the TMR (b) as a function of the bias voltage V and the position of the dots' levels $\varepsilon \equiv \varepsilon_1 = \varepsilon_2$ for double quantum dots coupled in parallel. The parameters are the same as in Fig. 2 with $\Gamma_{rj} \equiv \Gamma/2$, for $r = L, R$, $j = 1, 2$, and $\Gamma = 0.1$ meV. The transport regime where the Fano factor is divergent is marked with a thick black line.

VI. T-SHAPED DOUBLE QUANTUM DOTS

An interesting situation occurs when only one of the two quantum dots is coupled to external leads, while the other one is decoupled. In such T-shaped systems transport takes place through the molecular states of the double dot, although only the first dot is directly coupled to the leads. This may lead to new transport behavior, especially to a large super-Poissonian shot noise and an enhanced TMR, as we show in the sequel.

In Fig. 10 we present the current, differential conductance, the TMR and the Fano factor as a function of the bias voltage for the case when the first dot is coupled to the leads while the second dot is decoupled. Spin-dependent transport through single quantum dots have already been extensively studied. However, the hopping

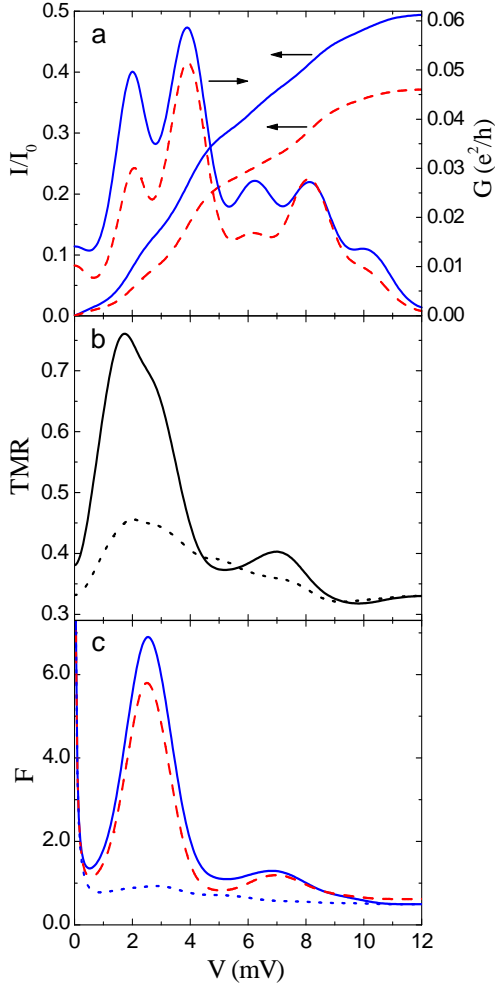


FIG. 10: (Color online) The bias dependence of the current and differential conductance (a), the TMR (b), and the Fano factor (c) in the parallel (solid line) and antiparallel (dashed line) configurations for T-shaped double quantum dots. The parameters are: $\Gamma_{r1} \equiv \Gamma/2$, and $\Gamma_{r2} = 0$ for $r = L, R$, with $\Gamma = 0.1$ meV, and $\varepsilon_1 = 1$ meV, $\varepsilon_2 = 0$ meV, $k_B T = 0.18$ meV, $U = 2$ meV, $U' = 1$ meV, $t = 0.2$ meV, and $p = 0.5$. The dotted curves present the TMR (b) and the Fano factor in the parallel configuration (c) calculated for $\Gamma_{r2} = \Gamma_{r1}$.

t between the two dots may modify the transport properties significantly, giving rise to novel behavior. First of all, we note that due to the finite t , transport takes place through molecular states of the double dot. This in turn leads to additional steps in the i - v curves and peaks in the differential conductance, see Fig. 10(a), as compared to tunneling through one single-level quantum dots, where for spin-degenerate level the current exhibits only two steps. The difference between the currents in the parallel and antiparallel configurations gives rise to the TMR which is shown in Fig. 10(b). The TMR displays an oscillatory-like behavior with increasing the bias voltage. In addition, at the threshold for sequential tunneling, the TMR becomes increased above the Julliere TMR.³⁷ This result is rather counterintuitive, as the Julliere TMR is

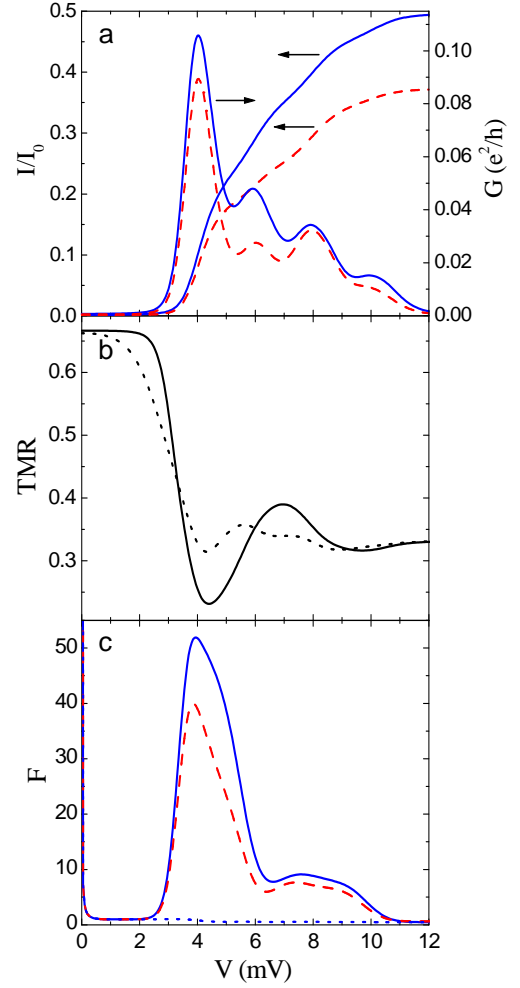


FIG. 11: (Color online) The bias dependence of the current, differential conductance (a), TMR (b) and the Fano factor (c) in the parallel (solid line) and antiparallel (dashed line) configurations. The parameters are the same as in Fig. 10 with $\varepsilon_2 = -4$ meV. The dotted curves present the TMR (b) and the Fano factor in the parallel configuration (c) calculated for $\Gamma_{r2} = \Gamma_{r1}$.

characteristic of a single ferromagnetic tunnel junction and one would expect that an additional object (quantum dot) between the leads should decrease the TMR. This was shown for single quantum dots with spin degenerate levels and symmetric couplings to the leads where the TMR was found to take at most the Julliere value.⁴³ In principle, the TMR can be enhanced above the Julliere value when only one spin component of the dot takes part in transport. Such spin selection may be achieved upon applying an external magnetic field or due to finite exchange interaction between spins in the dot.^{46,86} In the case of T-shaped DQDs, we find that the enhancement of the TMR is associated with increased occupation of the second dot in the antiparallel configuration, as compared to the parallel. Because the second dot is decoupled from the leads, this increases the difference between the current in the two configurations, yielding the TMR larger

than the Julliere value. In addition, finite occupation of the decoupled dot also leads to large current fluctuations, as the rate for tunneling between the second dot is much slower than that for tunneling between the first dot and the leads. This in turn gives rise to super-Poissonian shot noise, as displayed in Fig. 10(c). The super-Poissonian shot noise is present in both magnetic configurations. It is also slightly larger in the parallel configuration than in the antiparallel one, which is due to an additional contribution to the noise coming from spin-dependent tunneling between the dots and the leads.⁵⁴ We note that the super-Poissonian shot noise in T-shaped dots has also been reported in the case of nonmagnetic leads.⁸⁷ The two dots were however rather weakly coupled to each other so that no molecular states were formed, contrary to the case considered here.

The enhancement of the TMR above the Julliere value and the large super-Poissonian shot noise are present approximately at the threshold for sequential tunneling. In this transport regime the current is mainly mediated through the charge states of the decoupled dot. The aforementioned effects should therefore become washed out if there were a finite coupling between the second dot and the leads. This is shown in Fig. 10(b) and (c) where we depict the TMR and Fano factor in the parallel configuration calculated for $\Gamma_{r2} = \Gamma_{r1}$ (see the dotted curves in Fig. 10). The TMR larger than the Julliere TMR accompanied by super-Poissonian shot noise is thus an indication that transport takes place through quantum dot coupled to another dot, which is not connected to the leads directly.

Figure 11 displays the bias dependence of the current, TMR and the Fano factor calculated in the case when at equilibrium the second dot is fully occupied while the first dot is empty. At low bias voltage, the system is in the Coulomb blockade and the double dot is occupied with two electrons in the second dot with unit probability. The current flows then only due to elastic cotunneling processes. This gives rise to the Julliere TMR and Poissonian shot noise, see Fig. 11(b) and (c). With increasing the bias voltage, close to the threshold for sequential tunneling, the occupation of the second dot is slightly lowered at the cost of a finite occupation of another states. This opens the system for the cotunneling-assisted sequential and sequential tunneling processes. Nevertheless, because the double dot is still mainly occupied by two electrons on the decoupled dot, this gives rise to extremely large current fluctuations and Fano factors, see Fig. 11(c). This super-Poissonian shot noise can be considerably reduced once the second dot becomes coupled to the leads, see the dotted curve in Fig. 11(c).

Finally, in Fig. 12 we present the differential conductance in the parallel configuration and the TMR as a function of the bias voltage and the position of the second dot level. The Coulomb blockade regimes are clearly visible in Fig. 12(a), whereas the different behavior of the TMR depending on the transport regime is presented in Fig. 12(b).

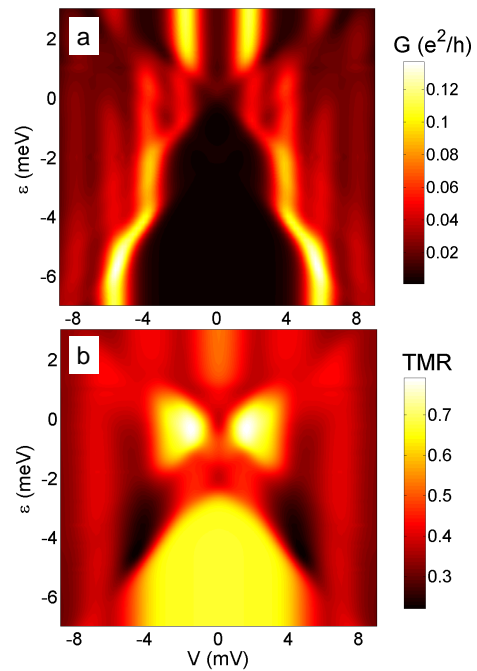


FIG. 12: (Color online) The differential conductance (a) in the parallel magnetic configuration, and the TMR (b) as a function of the bias voltage V and the position of the second dot level $\varepsilon \equiv \varepsilon_2$ for T-shaped double quantum dots. The parameters are the same as in Fig. 10.

VII. CONCLUSIONS

We have analyzed the spin-dependent transport through systems built of two strongly coupled quantum dots which are weakly connected to external ferromagnetic leads. The considerations were based on the real-time diagrammatic technique which allowed us to determine transport properties in the sequential and cotunneling regimes in a fully systematic way. In particular, we have analyzed the current, differential conductance, shot noise and the TMR for different geometries of the double dot system, including the serial and parallel couplings, as well as the T-shaped systems. We have also discussed the main differences in transport characteristics corresponding to different DQDs geometries, which may be helpful in determining the geometry of coupled quantum dots in experiments.

In the case of double quantum dots coupled in series, we have found an interesting dependence of the TMR on the occupation number of the DQD. Furthermore, the super-Poissonian shot noise in the Coulomb blockade regimes have been observed. On the other hand, when the levels of the DQD were detuned, transport characteristics revealed the Pauli spin blockade effects. We have shown that the leakage current, observed experimentally in the blockade regime,⁶ results from the interplay of cotunneling processes which flip the spin in the DQD and make the sequential tunneling possible. Thus, the current in the spin blockade flows due to cotunneling and spin-

flip cotunneling-assisted sequential tunneling processes. This mechanism is associated with pure nature of tunneling processes and is thus relevant for both nonmagnetic and ferromagnetic leads. In addition, we have also shown that the shot noise in the Pauli spin blockade regime becomes super-Poissonian, while outside the blockade it is sub-Poissonian.

For double quantum dots coupled in parallel, transport characteristics were found to be qualitatively similar to those in the case of DQDs coupled in series. The main difference is in the magnitude of conductance – for parallel DQDs it is roughly two times larger than for serial DQDs.

In addition, we have also analyzed the case when the first quantum dot is coupled to the leads while the second one is completely decoupled. In such T-shaped systems we have found a large super-Poissonian shot noise at the threshold for sequential tunneling and the TMR enhanced above the Julliere value. These effects are associated with an increased occupation of the decoupled quantum dot, and become washed out once there is a finite coupling between the second dot and the leads. Thus, the enhanced TMR together with large super-Poissonian shot noise may be an indication that transport takes place through quantum dot which is side-coupled to another

dot disconnected from the leads.

Acknowledgments

We acknowledge fruitful discussions with J. Barnaś. This work was supported by the Foundation for Polish Science and, as part of the European Science Foundation EUROCORES Programme SPINTRA, by funds from the Ministry of Science and Higher Education as a research project in years 2006-2009.

APPENDIX A: DETAILS OF NUMERICAL CALCULATIONS

In order to calculate the transport properties in the sequential and cotunneling regimes, it is necessary to find the elements of the respective first-order and second-order self-energy matrices. This can be done using the respective diagrammatic rules.^{43,75,76} Here, as an example, we present the contribution coming from $W_{\chi(N),\chi'(N)}^{(2)}$ where N is the charge state of the double dot. It is given by

$$\begin{aligned}
 W_{\chi(N),\chi'(N)}^{(2)} = & -2\pi \sum_{r,r'} \sum_{j,j'} \sum_{\sigma,\sigma'} \sum_{\chi''} \left\{ |\langle \chi | U^\dagger d_{j\sigma} U | \chi'' \rangle|^2 |\langle \chi'' | U^\dagger d_{j'\sigma'}^\dagger U | \chi' \rangle|^2 \left[\gamma_{rj}^{\sigma+}(\varepsilon_{\chi''} - \varepsilon_\chi) B_{2r'j'}^{\sigma'-}(\varepsilon_{\chi''} - \varepsilon_{\chi'}) \right. \right. \\
 & + \gamma_{r'j'}^{\sigma'+}(\varepsilon_{\chi''} - \varepsilon_{\chi'}) B_{2rj}^{\sigma+}(\varepsilon_{\chi''} - \varepsilon_\chi) - B_{2rj'j'}^{\sigma+\sigma'-}(\varepsilon_{\chi''} - \varepsilon_\chi, \varepsilon_{\chi'} - \varepsilon_\chi) \Big] \\
 & + |\langle \chi | U^\dagger d_{j\sigma}^\dagger U | \chi'' \rangle|^2 |\langle \chi'' | U^\dagger d_{j'\sigma'} U | \chi' \rangle|^2 \left[\gamma_{rj}^{\sigma-}(\varepsilon_\chi - \varepsilon_{\chi''}) B_{2r'j'}^{\sigma'+}(\varepsilon_{\chi'} - \varepsilon_{\chi''}) \right. \\
 & + \gamma_{r'j'}^{\sigma'+}(\varepsilon_{\chi'} - \varepsilon_{\chi''}) B_{2rj}^{\sigma-}(\varepsilon_\chi - \varepsilon_{\chi''}) - B_{2rj'j'}^{\sigma-\sigma'+}(\varepsilon_\chi - \varepsilon_{\chi''}, \varepsilon_\chi - \varepsilon_{\chi'}) \Big] \\
 & + \sum_{\chi'''} \langle \chi | U^\dagger d_{j\sigma}^\dagger U | \chi''' \rangle \langle \chi''' | U^\dagger d_{j'\sigma'} U | \chi' \rangle \langle \chi | U^\dagger d_{j'\sigma'} U | \chi'' \rangle \langle \chi'' | U^\dagger d_{j\sigma}^\dagger U | \chi' \rangle \times \\
 & \frac{2}{\varepsilon_\chi + \varepsilon_{\chi'} - \varepsilon_{\chi''} - \varepsilon_{\chi'''}} \left[B_{1rj'j'}^{\sigma-\sigma'+}(\varepsilon_{\chi''} - \varepsilon_{\chi'}, \varepsilon_\chi - \varepsilon_{\chi'}) - B_{1rj'j'}^{\sigma-\sigma'+}(\varepsilon_\chi - \varepsilon_{\chi''}, \varepsilon_\chi - \varepsilon_{\chi'}) \right] \Big\}, \quad (A1)
 \end{aligned}$$

where $\gamma_{rj}^{\sigma\pm}(\varepsilon) = \Gamma_{rj}^\sigma f^\pm(\varepsilon - \mu_r)/(2\pi)$, with f^+ being the Fermi distribution function, $f^- = 1 - f^+$, μ_r denoting the electrochemical potential of the lead r , and

$$\begin{aligned}
 B_{2rj}^{\sigma\pm}(\varepsilon) &= \int d\omega \frac{\gamma_{rj}^{\sigma\pm}(\omega)}{(\omega - \varepsilon)^2}, \\
 B_{\eta r j r' j'}^{\sigma\pm\sigma'\mp}(\varepsilon, \varepsilon') &= \int d\omega \gamma_{rj}^{\sigma\pm}(\omega) \gamma_{r'j'}^{\sigma'\mp}(\omega - \varepsilon') \frac{1}{(\omega - \varepsilon)^\eta}.
 \end{aligned}$$

We note that having found all the first-order and second-order self-energy matrices, we are in principle able to

calculate transport through arbitrary number of different orbital levels coupled to each other and to external leads in an arbitrary way. As far as numerical details are concerned, for systems consisting of larger number of orbital levels, in calculations we make use of the block structure of the initial Hamiltonian in the charge space, and perform unitary transformation of the Hamiltonian and the relevant local operators for each block separately. In addition, we also store the respective matrix elements in blocks labelled by charge quantum numbers.

-
- * Electronic address: weymann@amu.edu.pl
- ¹ F. R. Waugh, M. J. Berry, D. J. Mar, R. M. Westervelt, K. L. Campman, and A. C. Gossard, Phys. Rev. Lett. **75**, 705 (1995).
 - ² J. J. Palacios and P. Hawrylak, Phys. Rev. B **51**, 1769 (1995).
 - ³ R. H. Blick, R. J. Haug, J. Weis, D. Pfannkuche, K. v. Klitzing, and K. Eberl, Phys. Rev. B **53**, 7899 (1996).
 - ⁴ H. Imamura, H. Aoki, and P. A. Maksym, Phys. Rev. B **57**, R4257 (1998).
 - ⁵ R. Ziegler, C. Bruder, and H. Schoeller, Phys. Rev. B **62**, 1961 (2000).
 - ⁶ K. Ono, D. G. Austing, Y. Tokura, and S. Tarucha, Science **297**, 1313 (2002).
 - ⁷ W. G. van der Wiel, S. De Franceschi, J. M. Elzerman, T. Fujisawa, S. Tarucha, and L. P. Kouwenhoven, Rev. Mod. Phys. **75**, 1 (2003).
 - ⁸ H. W. Liu, T. Fujisawa, T. Hayashi, and Y. Hirayama, Phys. Rev. B **72**, 161305(R) (2005).
 - ⁹ V. N. Golovach and D. Loss, Phys. Rev. B **69**, 245327 (2004).
 - ¹⁰ D. T. McClure, L. DiCarlo, Y. Zhang, H.-A. Engel, C. M. Marcus, M. P. Hanson, and A. C. Gossard, Phys. Rev. Lett. **98**, 056801 (2007).
 - ¹¹ B. Wunsch, M. Braun, J. König, and D. Pfannkuche, Phys. Rev. B **72**, 205319 (2005).
 - ¹² M. R. Gräber, W. A. Coish, C. Hoffmann, M. Weiss, J. Furer, S. Oberholzer, D. Loss, and C. Schönenberger, Phys. Rev. B **74**, 075427 (2006).
 - ¹³ E. Cota, R. Aguado, and G. Platero, Phys. Rev. Lett. **94**, 107202 (2005).
 - ¹⁴ B. L. Hazelzet, M. R. Wegewijs, T. H. Stoof, and Yu. V. Nazarov, Phys. Rev. B **63**, 165313 (2001).
 - ¹⁵ J. Fransson, M. Rasander, Phys. Rev. B **73**, 205333 (2006).
 - ¹⁶ J. Fransson, Nanotechnology **17**, 5344 (2006); New J. Phys. **8**, 114 (2006).
 - ¹⁷ J. Inarrea, G. Platero and A. H. MacDonald, Phys. Rev. B **76**, 085329 (2007).
 - ¹⁸ B. Muralidharan and S. Datta, Phys. Rev. B **76**, 035432 (2007).
 - ¹⁹ P. Barthold, F. Hohls, N. Maire, K. Pierz, and R. J. Haug, Phys. Rev. Lett. **96**, 246804 (2006).
 - ²⁰ G. Kießlich, E. Schöll, T. Brandes, F. Hohls, and R. J. Haug, Phys. Rev. Lett. **99**, 206602 (2006).
 - ²¹ J. Aghassi, A. Thielmann, M. H. Hettler, and G. Schön, Phys. Rev. B **73**, 195323 (2006).
 - ²² P. Trocha, J. Barnaś, Phys. Rev. B **76**, 165432 (2007).
 - ²³ I. Weymann, Phys. Rev. B **75**, 195339 (2007).
 - ²⁴ J. N. Pedersen, B. Lassen, A. Wacker, and M. H. Hettler, Phys. Rev. B **75**, 235314 (2007).
 - ²⁵ S. A. Wolf, D. D. Awschalom, R. A. Buhrman, J. M. Daughton, S. von Molnar, M. L. Roukes, A. Y. Chtchelka, and D. M. Treger, Science **294**, 1488 (2001).
 - ²⁶ *Semiconductor Spintronics and Quantum Computation*, ed. by D.D. Awschalom, D. Loss, and N. Samarth (Springer, Berlin 2002).
 - ²⁷ S. Maekawa and T. Shinjo, *Spin Dependent Transport in Magnetic Nanostructures* (Taylor & Francis, New York 2002).
 - ²⁸ I. Zutic, J. Fabian, S. Das Sarma, Rev. Mod. Phys. **76**, 323 (2004).
 - ²⁹ S. Maekawa, *Concepts in Spin Electronics* (Oxford University Press, 2006).
 - ³⁰ R. Aguado and D. C. Langreth, Phys. Rev. Lett. **85**, 1946 (2000).
 - ³¹ R. Lopez, R. Aguado, and G. Platero, Phys. Rev. Lett. **89**, 136802 (2002).
 - ³² J. C. Chen, A. M. Chang, and M. R. Melloch, Phys. Rev. Lett. **92**, 176801 (2004).
 - ³³ D. Loss and D. P. DiVincenzo, Phys. Rev. A **57**, 120 (1998).
 - ³⁴ D. Loss and E. V. Sukhorukov, Phys. Rev. Lett. **84**, 1035 (2000).
 - ³⁵ X. Hu and S. Das Sarma, Phys. Rev. A **61**, 062301 (2000).
 - ³⁶ R. Hanson and G. Burkard, Phys. Rev. Lett. **98**, 050502 (2007).
 - ³⁷ M. Julliere, Phys. Lett. A **54**, 225 (1975).
 - ³⁸ J. Barnaś and A. Fert, Phys. Rev. Lett. **80**, 1058 (1998); S. Takahashi and S. Maekawa, Phys. Rev. Lett. **80**, 1758 (1998).
 - ³⁹ B. R. Buřka, Phys. Rev. B **62**, 1186 (2000).
 - ⁴⁰ W. Rudziński and J. Barnaś, Phys. Rev. B **64**, 085318 (2001).
 - ⁴¹ J. König and J. Martinek, Phys. Rev. Lett. **90**, 166602 (2003).
 - ⁴² M. Braun, J. König, J. Martinek, Phys. Rev. B **70**, 195345 (2004); Phys. Rev. B **74**, 075328 (2006).
 - ⁴³ I. Weymann, J. König, J. Martinek, J. Barnaś, and G. Schön, Phys. Rev. B **72**, 115334 (2005).
 - ⁴⁴ I. Weymann, J. Barnaś, J. König, J. Martinek, and G. Schön, Phys. Rev. B **72**, 113301 (2005).
 - ⁴⁵ S. Braig and P. W. Brouwer, Phys. Rev. B **71**, 195324 (2005).
 - ⁴⁶ I. Weymann, J. Barnaś, Phys. Rev. B **73**, 205309 (2006); Phys. Rev. B **75**, 155308 (2007); Eur. Phys. J. B **46**, 289 (2005); I. Weymann, Europhys. Lett. **76**, 1200 (2006).
 - ⁴⁷ F. M. Souza, J. C. Egues, and A. P. Jauho, Phys. Rev. B **75**, 165303 (2007).
 - ⁴⁸ J. Fransson, Europhys. Lett. **70**, 796 (2005).
 - ⁴⁹ A. Cottet, W. Belzig, and C. Bruder, Phys. Rev. B **70**, 115315 (2004); Phys. Rev. Lett. **92**, 206801 (2004).
 - ⁵⁰ A. Cottet and M.-S. Choi, Phys. Rev. B **74**, 235316 (2006).
 - ⁵¹ J. Martinek, Y. Utsumi, H. Imamura, J. Barnaś, S. Maekawa, J. König, and G. Schön, Phys. Rev. Lett. **91**, 127203 (2003); M.-S. Choi, D. Sanchez, and R. Lopez, Phys. Rev. Lett. **92**, 056601 (2004).
 - ⁵² Y. Utsumi, J. Martinek, G. Schön, H. Imamura, and S. Maekawa, Phys. Rev. B **71**, 245116 (2005).
 - ⁵³ M. Sindel, L. Borda, J. Martinek, R. Bulla, J. König, G. Schön, S. Maekawa, and J. von Delft, Phys. Rev. B **76**, 045321 (2007).
 - ⁵⁴ I. Weymann and J. Barnaś, Phys. Rev. B **77**, 075305 (2008).
 - ⁵⁵ R. Hornberger, S. Koller, G. Begemann, A. Donarini, and M. Grifoni, cond-mat/0712.0757 (unpublished).
 - ⁵⁶ J. R. Petta, A. C. Johnson, C. M. Marcus, M. P. Hanson, and A. C. Gossard, Phys. Rev. Lett. **93**, 186802 (2004).
 - ⁵⁷ A. C. Johnson, J. R. Petta, and C. M. Marcus, M. P. Hanson and A. C. Gossard, Phys. Rev. B **72**, 165308 (2005).
 - ⁵⁸ H. I. Jorgensen, K. Grove-Rasmussen, J. R. Hauptmann, P. E. Lindelof, Appl. Phys. Lett. **89** 232113 (2006).
 - ⁵⁹ S. Sapmaz, C. Meyer, P. Beliczynski, P. Jarillo-Herrero,

- Leo P. Kouwenhoven, *Nano Lett.* **6** (7), 1350 (2006).
- ⁶⁰ M. R. Gräber, M. Weiss, C. Schönenberger, *Semicond. Sci. Technol.* **21**, 64 (2006).
- ⁶¹ Y. Chye, M. E. White, E. Johnston-Halperin, B. D. Gerardot, D. D. Awschalom, and P. M. Petroff, *Phys. Rev. B* **66**, 201301(R) (2002).
- ⁶² H. B. Heersche, Z. de Groot, J. A. Folk, L. P. Kouwenhoven, and H. S. J. van der Zant, A. A. Houck, J. Labaziewicz, and I. L. Chuang, *Phys. Rev. Lett.* **96**, 017205 (2006).
- ⁶³ L. Y. Zhang, C. Y. Wang, Y. G. Wei, X. Y. Liu, and D. Davidović, *Phys. Rev. B* **72**, 155445 (2005).
- ⁶⁴ K. Tsukagoshi, B. W. Alphenaar, and H. Ago, *Nature* **401**, 572 (1999).
- ⁶⁵ B. Zhao, I. Mönch, H. Vinzelberg, T. Mühl, and C. M. Schneider, *Appl. Phys. Lett.* **80**, 3144 (2002).
- ⁶⁶ A. Jensen, J. R. Hauptmann, J. Nygard, and P. E. Lindelof, *Phys. Rev. B* **72**, 035419 (2005).
- ⁶⁷ S. Sahoo, T. Kontos, J. Furer, C. Hoffmann, M. Gräber, A. Cottet, and C. Schönenberger, *Nature Physics* **1**, 102 (2005).
- ⁶⁸ A. N. Pasupathy, R. C. Bialczak, J. Martinek, J. E. Grose, L. A. K. Donev, P. L. McEuen, and D. C. Ralph, *Science* **306**, 86 (2004).
- ⁶⁹ A. Bernand-Mantel, P. Seneor, N. Lidgi, M. Munoz, V. Cros, S. Fusil, K. Bouzehouane, C. Deranlot, A. Vaures, F. Petroff, and A. Fert, *Appl. Phys. Lett.* **89**, 062502 (2006).
- ⁷⁰ K. Hamaya, S. Masubuchi, M. Kawamura, T. Machida, M. Jung, K. Shibata, K. Hirakawa, T. Taniyama, S. Ishida, and Y. Arakawa, *Appl. Phys. Lett.* **90**, 053108 (2007).
- ⁷¹ K. Hamaya, M. Kitabatake, K. Shibata, M. Jung, M. Kawamura, K. Hirakawa, T. Machida, T. Taniyama, S. Ishida, and Y. Arakawa, *Appl. Phys. Lett.* **91**, 22107 (2007); *Appl. Phys. Lett.* **91**, 232105 (2007).
- ⁷² K. Hamaya, M. Kitabatake, K. Shibata, M. Jung, M. Kawamura, S. Ishida, T. Taniyama, K. Hirakawa, Y. Arakawa, and T. Machida, *Phys. Rev. B* **77**, 081302(R) (2008).
- ⁷³ H. Yang, S.-H. Yang, S. S. P. Parkin, *Nano Lett.* **8**, 340 (2008).
- ⁷⁴ B. R. Bulka and T. Kostyrko, *Phys. Rev. B* **70**, 205333 (2004).
- ⁷⁵ H. Schoeller and G. Schön, *Phys. Rev. B* **50**, 18436 (1994); J. König, J. Schmid, H. Schoeller, and G. Schön, *Phys. Rev. B* **54**, 16820 (1996).
- ⁷⁶ A. Thielmann, M. H. Hettler, J. König, and G. Schön, *Phys. Rev. Lett.* **95**, 146806 (2005); *Phys. Rev. B* **68**, 115105 (2003).
- ⁷⁷ D. V. Averin and A. A. Odintsov, *Phys. Lett. A* **140**, 251 (1989); D. V. Averin and Yu. V. Nazarov, *Phys. Rev. Lett.* **65**, 2446 (1990).
- ⁷⁸ K. Kang and B. I. Min, *Phys. Rev. B* **55**, 15412 (1997).
- ⁷⁹ D. V. Averin and Yu. V. Nazarov, in *Single Charge Tunneling*, edited by H. Grabert and M. Devoret (Plenum, New York 1992).
- ⁸⁰ Ya. M. Blanter and M. Büttiker, *Phys. Rep.* **336**, 1 (2000).
- ⁸¹ E. V. Sukhorukov, G. Burkard, and D. Loss, *Phys. Rev. B* **63**, 125315 (2001).
- ⁸² R. Hanson, L. P. Kouwenhoven, J. R. Petta, S. Tarucha, L. M. K. Vandersypen, *Rev. Mod. Phys.* **79**, 1217 (2007).
- ⁸³ K. Ono and S. Tarucha, *Phys. Rev. Lett.* **92**, 256803 (2004).
- ⁸⁴ A. Kogan, S. Amasha, D. Goldhaber-Gordon, G. Granger, M. A. Kastner, and H. Shtrikman, *Phys. Rev. Lett.* **93**, 166602 (2004).
- ⁸⁵ A. W. Holleitner, A. Chudnovskiy, D. Pfannkuche, K. Eberl, and R. H. Blick, *Phys. Rev. B* **70**, 075204 (2004).
- ⁸⁶ I. Weymann and J. Barnaś, *J. Phys.: Condens. Matter* **19**, 096208 (2007).
- ⁸⁷ I. Djuric, B. Dong, H. L. Cui, *Appl. Phys. Lett.* **87**, 032105 (2005).

Effects of different geometries on the conductance, shot noise and tunnel magnetoresistance of double quantum dots

Ireneusz Weymann^{1, 2, *}

¹*Department of Physics, Adam Mickiewicz University, 61-614 Poznań, Poland*

²*Department of Theoretical Physics, Institute of Physics,
Budapest University of Technology and Economics, H-1521 Budapest, Hungary*

(Dated: October 30, 2018)

The spin-polarized transport through a coherent strongly coupled double quantum dot (DQD) system is analyzed theoretically in the sequential and cotunneling regimes. Using the real-time diagrammatic technique, we analyze the current, differential conductance, shot noise and tunnel magnetoresistance (TMR) as a function of both the bias and gate voltages for double quantum dots coupled in series, in parallel as well as for T-shaped systems. For DQDs coupled in series, we find a strong dependence of the TMR on the number of electrons occupying the double dot, and super-Poissonian shot noise in the Coulomb blockade regime. In addition, for asymmetric DQDs, we analyze transport in the Pauli spin blockade regime and explain the existence of the leakage current in terms of cotunneling and spin-flip cotunneling-assisted sequential tunneling. For DQDs coupled in parallel, we show that the transport characteristics in the weak coupling regime are qualitatively similar to those of DQDs coupled in series. On the other hand, in the case of T-shaped quantum dots and predict a large super-Poissonian shot noise and TMR enhanced above the Julliere value due to increased occupation of the decoupled quantum dot. We also discuss the possibility of determining the geometry of the double dot from transport characteristics. Furthermore, where possible, we compare our results with existing experimental data on nonmagnetic systems and find qualitative agreement.

PACS numbers: 72.25.Mk, 73.63.Kv, 85.75.-d, 73.23.Hk

I. INTRODUCTION

Transport properties of double quantum dots (DQDs) have recently attracted much interest.^{1,2,3,4,5,6,7,8,9,10,11,12,13,14,15,16,17,18,19,20,21,22,23,24} Since the behavior of double quantum dots resembles the behavior of molecules, DQDs are frequently called *artificial molecules*, and are thus considered as ideal systems to study the fundamental many-body interactions between single electrons and spins.^{25,26,27,28,29} Double quantum dots exhibit a variety of interesting effects, such as for example current rectification due to the Pauli spin blockade,^{4,6,15,16,17,18} negative differential conductance,⁸ formation of molecular states,^{2,3,12} spin pumping,^{13,14} Kondo effect,^{30,31,32} etc. Furthermore, double quantum dots are also interesting for future applications in quantum computing.^{33,34,35,36} In addition, when the leads are ferromagnetic, transport properties of the system strongly depend on the relative orientation of the magnetizations of electrodes, leading to the tunnel magnetoresistance (TMR) effect, spin accumulation, exchange field, etc.^{22,23,37,38,39,40,41,42,43}

The problem of spin-polarized transport properties has been so far mainly addressed in the case of single quantum dots.^{39,40,41,42,43,44,45,46,47,48,49,50,51,52,53,54} In particular, in the strong coupling regime it was shown that the Kondo peak becomes split when the magnetic configuration changes from the antiparallel to parallel one, and that this splitting can be compensated upon applying external magnetic field.^{51,52,53} In the weak coupling regime, on the other hand, the parity effect of the linear response

TMR was predicted⁴³ and the zero-bias anomaly was found in the differential conductance when magnetic moments of the leads form an antiparallel configuration.⁴⁴ In this paper we extend the existing theoretical studies and consider transport through coherent double quantum dots weakly coupled to external ferromagnetic leads. We note that spin-dependent transport properties of DQDs have been analyzed very recently in a few theoretical papers.^{16,23,55} The considerations were however limited to either first-order tunneling or the Coulomb blockade regime. In particular, in Ref. [16] the formation of a pure triplet state was predicted, Ref. [23] deals with transport in the deep Coulomb blockade regime, while Ref. [55] presents a detailed analysis of sequential transport in the case of non-collinearly polarized leads.

The goal of this paper is thus to analyze the transport properties of double quantum dots coupled to collinear ferromagnetic leads in the full weak coupling regime, i.e. including sequential, cotunneling and cotunneling-assisted sequential processes. Furthermore, we also analyze the effect of different geometries of the double dots on transport, in particular, the cases of DQDs coupled in series, in parallel, as well as T-shaped double quantum dots are considered. The comparison of numerical results obtained for different geometries may in principle help in determining the system's geometry, which may be of importance in discussing and understanding experimental results, especially on self-assembled quantum dots. The present analysis is based on the real-time diagrammatic technique which consists in a perturbation expansion of the density matrix of the system under consideration,

and the relevant operators, with respect to the coupling to external leads. The advantage of using the real-time diagrammatic technique is that it takes into account the effects of the exchange field and the renormalization of the dot levels in a fully systematic way. In particular, in the case of asymmetric DQDs coupled in series, we consider transport in the Pauli spin blockade regime and show that the leakage current in the blockade region results from cotunneling and cotunneling-assisted sequential tunneling processes. As far as the shot noise is concerned, we show that the noise is super-Poissonian in the Coulomb blockade regime and drops to sub-Poissonian value in the sequential tunneling regime, where the Fano factor approaches one half. This behavior is observed for parallel and serial DQD's geometries. In turn, for T-shaped double quantum dots, we find a large super-Poissonian shot noise due to increased occupation of the decoupled dot. We also analyze the TMR effect and find its strong dependence on the transport regime and number of electrons in the DQD in the ground state. For DQDs coupled in series and in parallel the TMR takes the values ranging from around a half of the Julliere TMR to its full value,³⁷ whereas for T-shaped DQDs the TMR may be enhanced above the Julliere value.

The systems considered in this paper may be realized experimentally for example in lateral and vertical semiconductor quantum dots^{6,8,10,56,57} or single wall metallic carbon nanotubes with top gate electrodes.^{12,58,59,60} The latter systems are of particular interest because, by tuning the gates, it is possible to change the charge on each dot separately. Unfortunately, the aforementioned experiments concerned only DQDs coupled to nonmagnetic leads. There are several experimental realizations of single quantum dots attached to ferromagnetic leads,^{61,62,63,64,65,66,67,68,69,70,71,72,73} while experimental data on spin-polarized transport through double quantum dots are lacking. We thus believe that the results presented in this paper will be of assistance in discussing future experiments.

The paper is organized as follows: The model of the considered system is presented in Sec. II, whereas the method employed in calculations is described in Sec. III. In Section IV we present and discuss the numerical results for double quantum dots coupled in series. In this section we also focus on the role of second-order processes in transport. In addition, we also analyze transport in the Pauli spin blockade regime. In Sec. V we deal with DQDs coupled in parallel, whereas in Sec. VI we consider transport through T-shaped quantum dots. Finally, the conclusions are given in Sec. VII.

II. MODEL

The schematic of a double quantum dot coupled to ferromagnetic leads is shown in Fig. 1. It is assumed that the magnetizations of the leads are oriented collinearly, so that the system can be either in the parallel or an-

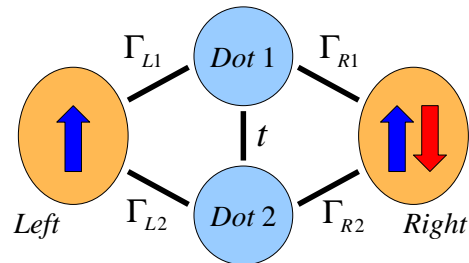


FIG. 1: (Color online) Schematic of a double quantum dot weakly coupled to external ferromagnetic electrodes. The magnetizations of the leads can form either parallel or antiparallel magnetic configuration. The first ($j = 1$) and second ($j = 2$) dots are coupled to each other via the hopping t , and to the left ($r = L$) and right ($r = R$) leads with the coupling strength Γ_{rj} . The double quantum dot is assumed to be symmetrically biased. By adjusting the couplings, the system can smoothly cross over from the serial to parallel geometry.

tiparallel magnetic configuration. The Hamiltonian of the system is given by

$$H = H_L + H_R + H_{\text{DQD}} + H_T \quad (1)$$

The first two terms describe noninteracting itinerant electrons in the leads, $H_r = \sum_{\mathbf{k}\sigma} \varepsilon_{r\mathbf{k}\sigma} c_{r\mathbf{k}\sigma}^\dagger c_{r\mathbf{k}\sigma}$ for the left ($r = L$) and right ($r = R$) lead, where $\varepsilon_{r\mathbf{k}\sigma}$ is the energy of an electron with the wave vector \mathbf{k} and spin σ in the lead r , and $c_{r\mathbf{k}\sigma}^\dagger$ ($c_{r\mathbf{k}\sigma}$) denotes the respective creation (annihilation) operator. The double dot is described by the Hamiltonian

$$H_{\text{DQD}} = \sum_{j=1,2} \sum_{\sigma} \varepsilon_j n_{j\sigma} + U \sum_{j=1,2} n_{j\uparrow} n_{j\downarrow} + U' \sum_{\sigma\sigma'} n_{1\sigma} n_{2\sigma'} + t \sum_{\sigma} (d_{1\sigma}^\dagger d_{2\sigma} + d_{2\sigma}^\dagger d_{1\sigma}), \quad (2)$$

with $n_{j\sigma} = d_{j\sigma}^\dagger d_{j\sigma}$, where $d_{j\sigma}^\dagger$ ($d_{j\sigma}$) is the creation (annihilation) operator of an electron with spin σ in the first ($j = 1$) or second ($j = 2$) quantum dot, and ε_j is the corresponding single-particle energy. The Coulomb interaction on the first and second dot is assumed to be equal and is described by U , while U' corresponds to the inter-dot Coulomb correlation. The last term of H_{DQD} describes the hopping between the two dots with t being the hopping parameter. We assume that the hopping parameter is large, so that there is a considerable overlap of the wave functions of the two dots, leading to the formation of molecular many-body states, through which transport takes place. In addition, we also note that an exchange interaction between spins in the two dots may lead to the formation of singlet and triplet states.¹² However, experimentally, this exchange interaction was found to be rather small as compared to the other energy scales,⁶ therefore, in the following considerations, we will neglect it.

The tunneling processes between the DQD and elec-

trodes are described by the Hamiltonian,

$$H_T = \sum_{r=L,R} \sum_{j=1,2} \sum_{\mathbf{k}\sigma} \left(t_{rj} c_{r\mathbf{k}\sigma}^\dagger d_{j\sigma} + t_{rj}^* d_{j\sigma}^\dagger c_{r\mathbf{k}\sigma} \right), \quad (3)$$

where t_{rj} denotes the tunnel matrix elements between the r th lead and the j th dot. The coupling of the j th dot to the r th lead can be written as $\Gamma_{rj}^\sigma = 2\pi |t_{rj}|^2 \rho_r^\sigma$, where ρ_r^σ is the spin-dependent density of states of lead r . By introducing the definition of the spin polarization of lead r , $p_r = (\rho_r^+ - \rho_r^-)/(\rho_r^+ + \rho_r^-)$, one can write, $\Gamma_{rj}^{+(-)} = \Gamma_{rj}(1 \pm p_r)$, with $\Gamma_{rj} = (\Gamma_{rj}^+ + \Gamma_{rj}^-)/2$, where Γ_{rj}^+ and Γ_{rj}^- describe the coupling of the j th dot to the spin-majority and spin-minority electron bands of the lead r , respectively.

Because the double dot Hamiltonian, Eq. (2), is not diagonal in the local basis, we perform a unitary transformation, $U^\dagger H_{\text{DQD}} U = \tilde{H}_{\text{DQD}}$, to a new basis in which \tilde{H}_{DQD} is diagonal, $\tilde{H}_{\text{DQD}}|\chi\rangle = \varepsilon_\chi|\chi\rangle$. The eigenvectors $|\chi\rangle$ are the many-body states of the double quantum dot, while the eigenvalues ε_χ denote the corresponding energies.⁷⁴

III. METHOD

In order to calculate the spin-dependent transport properties of a double quantum dot in the sequential and cotunneling regimes, we employ the real-time diagrammatic technique.^{43,75,76} It consists in a systematic perturbation expansion of the reduced density matrix of the considered system and the current operator with respect to the dot-lead coupling strength Γ . The time evolution of the reduced density matrix can be visualized as a sequence of irreducible self-energy blocks, $W_{\chi\chi'}$, on the Keldysh contour, where $W_{\chi\chi'}$ describe transitions between the many-body DQD states $|\chi\rangle$ and $|\chi'\rangle$. The elements $W_{\chi\chi'}$ set up a self-energy matrix \mathbf{W} . Within the matrix notation introduced by Thielmann *et al.*,⁷⁶ the stationary elements of the reduced density matrix can be found from

$$(\tilde{\mathbf{W}}\mathbf{p}^{\text{st}})_\chi = \Gamma\delta_{\chi\chi_0}, \quad (4)$$

where \mathbf{p}^{st} is the vector containing probabilities and the matrix $\tilde{\mathbf{W}}$ is the modified matrix \mathbf{W} so as to include the normalization of probabilities. The current flowing through the system can be then found from

$$I = \frac{e}{2\hbar} \text{Tr}\{\mathbf{W}^I \mathbf{p}^{\text{st}}\}. \quad (5)$$

The matrix \mathbf{W}^I is the self-energy matrix with one *internal* vertex resulting from the expansion of the tunneling Hamiltonian replaced by the current operator.

To calculate the transport properties order by order in tunneling processes, we expand the self-energy matrices, $\mathbf{W} = \mathbf{W}^{(1)} + \mathbf{W}^{(2)} + \dots$, $\mathbf{W}^I = \mathbf{W}^{I(1)} + \mathbf{W}^{I(2)} + \dots$, and

the dot occupations, $\mathbf{p}^{\text{st}} = \mathbf{p}^{\text{st}(0)} + \mathbf{p}^{\text{st}(1)} + \dots$, respectively. Then, the first-order (sequential) and the second-order (cotunneling) currents are given by

$$\begin{aligned} I^{(1)} &= \frac{e}{2\hbar} \text{Tr}\{\mathbf{W}^{I(1)} \mathbf{p}^{\text{st}(0)}\}, \\ I^{(2)} &= \frac{e}{2\hbar} \text{Tr}\{\mathbf{W}^{I(2)} \mathbf{p}^{\text{st}(0)} + \mathbf{W}^{I(1)} \mathbf{p}^{\text{st}(1)}\}. \end{aligned} \quad (6)$$

On the other hand, the zeroth and first-order occupation probabilities can be found from the following equations

$$\begin{aligned} (\tilde{\mathbf{W}}^{(1)} \mathbf{p}^{\text{st}(0)})_\chi &= \Gamma\delta_{\chi\chi_0}, \\ \tilde{\mathbf{W}}^{(1)} \mathbf{p}^{\text{st}(1)} + \tilde{\mathbf{W}}^{(2)} \mathbf{p}^{\text{st}(0)} &= 0, \end{aligned} \quad (7)$$

where $\tilde{\mathbf{W}}^{(1)} [\tilde{\mathbf{W}}^{(2)}]$ is given by $\mathbf{W}^{(1)} [\mathbf{W}^{(2)}]$ with one arbitrary row χ_0 replaced by (Γ, \dots, Γ) $[(0, \dots, 0)]$ due to the normalization of probabilities, $\sum_\chi p_\chi^{\text{st}(n)} = \delta_{n,0}$.

As one can see from the above formulas, to determine the transport properties it is necessary to calculate the elements of the corresponding self-energy matrices. This can be done using the respective diagrammatic rules.^{43,75,76} Although the first-order calculation is rather simple, the general analytical formulas for the self-energies in the second order are rather complicated due to many virtual states through which the cotunneling processes can take place. In the Appendix A, as an example, we present the contribution coming from $W_{\chi(N),\chi'(N)}^{(2)}$ where N is the charge state of the double dot.

In addition, in the present paper we also analyze the zero-frequency current noise of the double quantum dot system, $S = 2 \int_{-\infty}^0 dt (\langle \hat{I}(t) \hat{I}(0) + \hat{I}(0) \hat{I}(t) \rangle - 2\langle \hat{I} \rangle^2)$. For low bias voltages the current noise is dominated by thermal noise, while for $|eV| > k_B T$ the noise associated with the discrete nature of charge (shot noise) dominates.⁸⁰ Within the real-time diagrammatic technique, a general formula for the shot noise has been derived in Ref. [76] taking into account the non-Markovian effects. The shot noise in the first-order can be found from the corresponding expression

$$S^{(1)} = \frac{e^2}{\hbar} \text{Tr} \left[\left(\mathbf{W}^{\text{II}(1)} + \mathbf{W}^{I(1)} \mathbf{P}^{(-1)} \mathbf{W}^{I(1)} \right) \mathbf{p}^{\text{st}(0)} \right], \quad (8)$$

while the cotunneling current noise is given by

$$\begin{aligned} S^{(2)} &= \frac{e^2}{\hbar} \text{Tr} \left\{ \left[\mathbf{W}^{\text{II}(2)} + \mathbf{W}^{I(2)} \mathbf{P}^{(-1)} \mathbf{W}^{I(1)} \right. \right. \\ &\quad + \mathbf{W}^{I(1)} \mathbf{P}^{(-1)} \mathbf{W}^{I(2)} + \mathbf{W}^{I(1)} \mathbf{P}^{(0)} \mathbf{W}^{I(1)} \\ &\quad + \left. \left. \mathbf{W}^{I(1)} \mathbf{Q}^{(0)} \partial \mathbf{W}^{I(1)} \right] \mathbf{p}^{\text{st}(0)} \right. \\ &\quad + \left. \left[\mathbf{W}^{\text{II}(1)} + \mathbf{W}^{I(1)} \mathbf{P}^{(-1)} \mathbf{W}^{I(1)} \right] \mathbf{p}^{\text{st}(1)} \right\}, \end{aligned} \quad (9)$$

where $\mathbf{Q}^{(n)} = \mathbf{p}^{\text{st}(n)} \otimes \mathbf{e}^T$, with $\mathbf{e}^T = (1, \dots, 1)$. The objects $\mathbf{P}^{(-1)}$ and $\mathbf{P}^{(0)}$ are given by, $\tilde{\mathbf{W}}^{(1)} \mathbf{P}^{(-1)} = \mathbf{Q}^{(1)} - \mathbf{1}$, and, $\tilde{\mathbf{W}}^{(1)} \mathbf{P}^{(0)} + \tilde{\mathbf{W}}^{(2)} \mathbf{P}^{(-1)} = \tilde{\mathbf{1}}(\mathbf{Q}^{(1)} - \partial \mathbf{W}^{(1)} \mathbf{Q}^{(0)})$, respectively, with $\tilde{\mathbf{1}}$ being the unit vector with row χ_0 set to zero. On the other hand, the matrices $\mathbf{W}^{\text{II}(1)}$ and $\mathbf{W}^{\text{II}(2)}$

are the first and second-order self-energy matrices with two internal vertices replaced by the current operator, while $\partial \mathbf{W}^{(1)}$ and $\partial \mathbf{W}^{I(1)}$ are partial derivatives of $\mathbf{W}^{(1)}$ and $\mathbf{W}^{I(1)}$ with respect to the convergence factor of the Laplace transform.⁷⁶

By taking into account all the first-order and second-order contributions to the self-energies, we are able to resolve the transport properties in the full range of the bias and gate voltages. The first order of expansion with respect to the coupling corresponds to sequential tunneling, while the second order is associated with cotunneling. Sequential tunneling is allowed if the applied bias is larger than the threshold voltage, i.e. when the energy provided by the transport voltage is comparable with the charging energy. Otherwise, the system is in the Coulomb blockade regime where sequential tunneling is exponentially suppressed and the current flows due to cotunneling, which involves correlated tunneling through virtual states of the system.^{77,78,79}

Among different cotunneling processes one can generally distinguish two types of processes: non-spin-flip ones, which do not affect the DQD state, and the spin-flip ones. Furthermore, one can also have double-barrier cotunneling, which contributes directly to the current, and single-barrier cotunneling, which affects the double dot occupations and, thus, indirectly, the current.

IV. DOUBLE QUANTUM DOTS COUPLED IN SERIES

In this section we present and discuss numerical results on double quantum dots coupled in series. In order to realize this geometry we set $\Gamma_{L2} = \Gamma_{R1} = 0$ and assume $\Gamma_{L1} = \Gamma_{R2} \equiv \Gamma/2$, see Fig. 1. Furthermore, in the following we will also distinguish between symmetric and asymmetric DQDs. In the former case, the level position of each dot is the same, $\varepsilon_1 = \varepsilon_2$, while in the latter case the levels are detuned, $\varepsilon_1 \neq \varepsilon_2$. In addition, in this section we will emphasize the role of second-order processes in transport. In order to ascribe observed features to respective tunneling processes, we will therefore also present results obtained within the sequential tunneling approximation, i.e. when considering only the first-order tunneling processes.

A. Symmetric double quantum dots

The differential conductance as a function of the bias voltage and the position of the dot levels for the parallel and antiparallel configurations is shown in Fig. 2(a) and (b). Because experimentally the position of the dots' levels can be changed upon applying a gate voltage, Fig. 2 effectively shows the bias and gate voltage dependence of the conductance. First of all, it can be seen that the differential conductance displays a characteristic Coulomb diamond structure. The diamonds in the low bias volt-

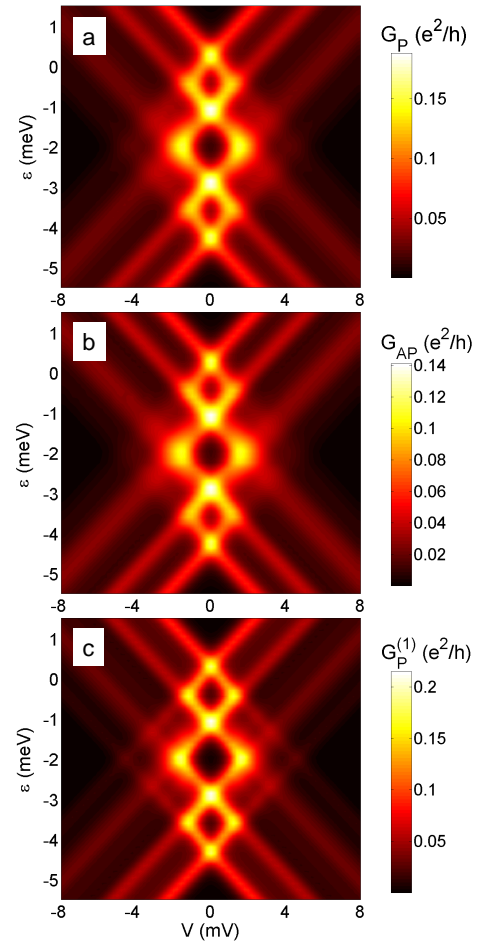


FIG. 2: (Color online) The differential conductance in the parallel G_P (a) and antiparallel G_{AP} (b) magnetic configurations as a function of the bias voltage V and the position of the dots' levels $\varepsilon \equiv \varepsilon_1 = \varepsilon_2$ for double quantum dots coupled in series. The parameters are: $k_B T = 0.15$ meV, $U = 2$ meV, $U' = 1$ meV, $t = 0.25$ meV, $\Gamma_{L2} = \Gamma_{R1} = 0$, $\Gamma_{L1} = \Gamma_{R2} \equiv \Gamma/2$, with $\Gamma = 0.1$ meV, and $p = 0.5$. Because the double quantum dot is symmetric, $\varepsilon_1 = \varepsilon_2$, there is no asymmetry associated with the bias reversal. For comparison in part (c) we also show the density plot of the differential conductance in the parallel configuration calculated using only the first-order tunneling processes, $G_P^{(1)}$.

age regime correspond to the Coulomb blockade regime where the sequential current is exponentially suppressed and the current flows due to cotunneling. With increasing the bias voltage the excited states start participating in transport, which leads to additional lines in the differential conductance. The features described above are rather associated with the energy spectrum and charge states of the DQD than with the ferromagnetism of the leads, therefore they are present in both magnetic configurations. The spin dependence stemming from ferromagnetic electrodes gives rise to a difference of the conductance in the parallel and antiparallel configurations, see Fig. 2(a) and (b). The conductance in the parallel

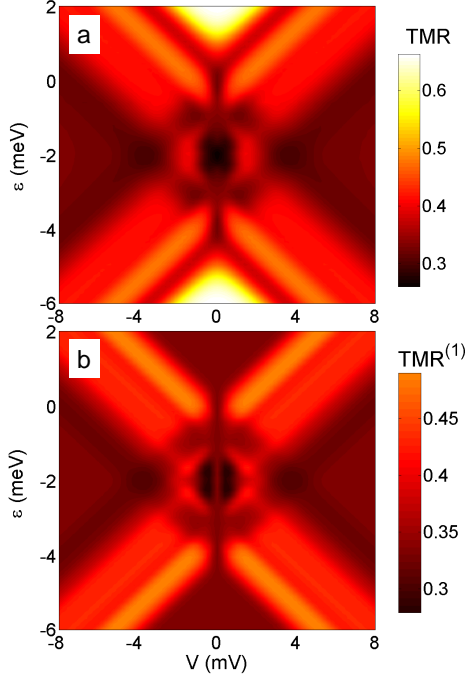


FIG. 3: (Color online) The total (first and second order) TMR (a) and the first-order TMR (b) as a function of the bias voltage V and the level position ε for parameters the same as in Fig. 2. The two figures are plotted in the same scale.

configuration is generally larger than that in the antiparallel configuration. This is due to the spin asymmetry in the couplings when the leads' magnetizations are antiparallel. As in the parallel configuration the majority (minority) electrons of, let us say, left lead tunnel to the majority (minority) electron band of the right lead, in the antiparallel configuration the situation is reversed – the majority (minority) electrons of the left lead tunnel to the minority (majority) electron band of the right lead. This leads to the difference of the conductance in both magnetic configurations, see Fig. 2, and to the corresponding tunnel magnetoresistance effect. In addition, in Fig. 2(c) we also present the bias and gate voltage dependence of the differential conductance for the parallel configuration calculated within the sequential tunneling approximation, $G_P^{(1)}$. By comparing Fig. 2(a) and (c), one can see that cotunneling leads to broadening of the resonance peaks, lowering the magnitude of the differential conductance, and gives rise to finite conductance in the Coulomb blockade regimes.

The bias and gate voltage dependence of the TMR is shown in Fig. 3(a), while Fig. 3(b) presents the first-order TMR, $\text{TMR}^{(1)}$. Intuitively, the TMR is a measure of the system's transport properties change when the magnetic configuration switches from the parallel to the antiparallel one. It is defined as^{37,38,43}

$$\text{TMR} = \frac{I_P - I_{AP}}{I_{AP}}, \quad (10)$$

where I_P (I_{AP}) is the current flowing through the sys-

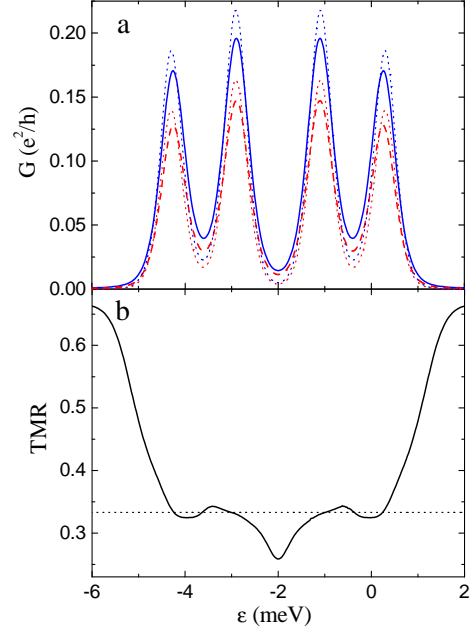


FIG. 4: (Color online) The linear conductance in the parallel (solid line) and antiparallel (dashed line) magnetic configurations (a) and the linear TMR (b) as a function of the level position ε for parameters the same as in Fig. 2. For comparison, the dotted curves show the linear conductance and the TMR calculated taking into account only the first-order processes.

tem in the parallel (antiparallel) configuration. By comparison with Fig. 2, one can easily identify the different transport regimes. Furthermore, by comparing the total and sequential TMR, one can immediately see that cotunneling modifies the TMR mainly in the low bias voltage regime, i.e. in the Coulomb blockade regime and in the regime where sequential tunneling is suppressed due to the absence of levels in the energy window provided by transport voltage. In order to discuss and see more clearly the behavior of the TMR on applied voltages, in Fig. 4 we show the linear response conductance and resulting TMR, while in Fig. 5 we display the transport properties in the nonlinear response regime.

The linear conductance in both magnetic configurations is shown in Fig. 4(a). When lowering the position of the DQD levels the conductance displays four resonance peaks associated with subsequent occupation of the corresponding charge states. The dotted curves in Fig. 4 present results obtained in the first-order approximation. It can be seen that off resonance the current is mainly dominated by cotunneling. On the other hand, on resonance the sequential processes dominate current, while cotunneling only slightly affects the conductance, leading to renormalization of the DQD levels and, thus, slightly shifting the position of the conductance peaks, see Fig. 4(a). Interestingly, the second-order processes have a rather large impact on the linear TMR shown in Fig. 4(b). First of all, the linear response TMR exhibits

a strong dependence on the gate voltage, i.e. on the number of electrons in the double quantum dot. When the DQD is either empty or fully occupied, the TMR is given by the Julliere value, $\text{TMR} = 2p^2/(1 - p^2)$.³⁷ This is due to the fact that in those transport regimes the current is driven by elastic cotunneling processes which do not affect the DQD state in any way. Thus, as far as the TMR is concerned, the system behaves as a single ferromagnetic tunnel junction.³⁷ However, in the Coulomb blockade regions, the TMR becomes generally suppressed due to the presence of inelastic cotunneling which introduces spin-flip processes in the system. The dotted line in Fig. 4(b) shows the TMR calculated within the sequential tunneling approximation – it is given by $\text{TMR} = p^2/(1 - p^2)$.^{43,55} At this point, we would like to note that the results for the linear conductance calculated by including only the first-order processes are rather reliable in the whole range of ε . On the other hand, the results for the linear response TMR are comparable to those obtained within the sequential tunneling approximation only on resonance, where sequential processes dominate, while off resonance they are completely unreliable, see Fig. 4. Therefore, in order to properly analyze the dependence of the TMR in the full range of parameters one has to take into account cotunneling processes.

The bias voltage dependence of the current, differential conductance, tunnel magnetoresistance and the Fano factor is shown in Fig. 5 for $\varepsilon = -2$ meV and $\varepsilon = 2$ meV. The first situation, $\varepsilon = -2$ meV, corresponds to the case when the ground state of the double quantum dot is doubly occupied, while the second one, $\varepsilon = 2$ meV, corresponds to the case of empty double dot. In all cases, due to the spin asymmetry of tunneling processes, the current in the parallel configuration is larger than the current in the antiparallel configuration. In addition, the i - v curves display characteristic Coulomb steps. With increasing the bias voltage more and more charge states start to participate in transport which gives rise to the corresponding steps in the current-voltage characteristics, and peaks in the differential conductance. Furthermore, the single-electron charging effects also lead to the oscillatory-like behavior of the TMR effect, see Fig. 5(c) and (g). In the Coulomb blockade regime, $\varepsilon = -2$ meV, the TMR is much suppressed as compared to the case of $\varepsilon = 2$ meV. This is due to the presence of spin-flip cotunneling processes in the case of the doubly occupied DQD, as already discussed in association with Fig. 4. However, when increasing the bias voltage the TMR increases and, at the threshold for sequential tunneling, reaches a local maximum, see Fig. 5(c). This effect is due to the nonequilibrium spin accumulation which is induced in the DQD system with increasing the transport voltage. (Similar effect can be observed when the double dot is singly occupied, i.e. when $\varepsilon = -0.5$ meV.) On the other hand, when the DQD is empty, the TMR at low bias voltage acquires the Julliere value,³⁷ and then, with increasing V , becomes generally suppressed, see Fig. 5(g).

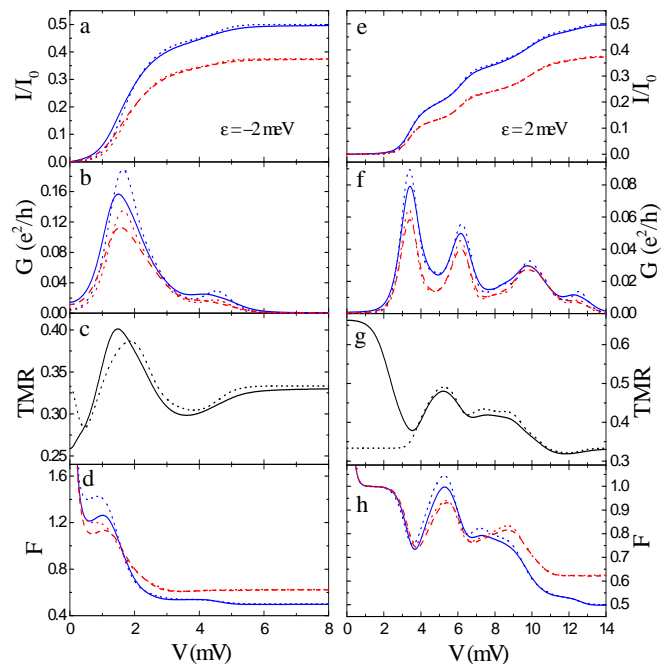


FIG. 5: (Color online) The current in units of $I_0 = e\Gamma/\hbar$ (a,e), differential conductance (b,f) and the Fano factor (d,h) in the parallel (solid line) and antiparallel configuration (dashed line) as well as the TMR (c,g) as a function of the bias voltage for different values of the level position ε as indicated in the figure. $\varepsilon = -2$ meV (a-d) corresponds to the case when the ground state of the DQD is doubly occupied, while for $\varepsilon = 2$ meV (e-h) the double dot is empty. The parameters are the same as in Fig. 2. The dotted curves show the results obtained in the sequential tunneling approximation.

In addition, in Fig. 5 we also show the Fano factor, $F = S/(2e|I|)$, calculated in both magnetic configurations and for two values of ε , as indicated in the figure. First of all, one can see that the Fano factor becomes divergent at low bias voltages. This is due to the thermal noise which dominates the current noise as $V \rightarrow 0$, while $I \rightarrow 0$, leading to $F \rightarrow \infty$.⁸⁰ Furthermore, it can be seen that the Fano factor in the Coulomb blockade regime is slightly larger in the parallel configuration than in the antiparallel one. This is associated with an additional positive cross-correlations, which contribute to the current noise, due to the ferromagnetism of the electrodes. In the Coulomb blockade regime, there is a larger asymmetry between the cotunneling processes through the majority and minority spin channels in the parallel configuration than in the antiparallel one. This effectively increases the current fluctuations in the parallel configuration and leads to the corresponding difference in the Fano factors, see Fig. 5(d). On the other hand, in the sequential tunneling regime, the information about the spin asymmetry of tunneling processes between the DQD and the corresponding lead is rather contained in the nonequilibrium spin accumulation induced in the double dot. This spin accumulation is larger in the an-

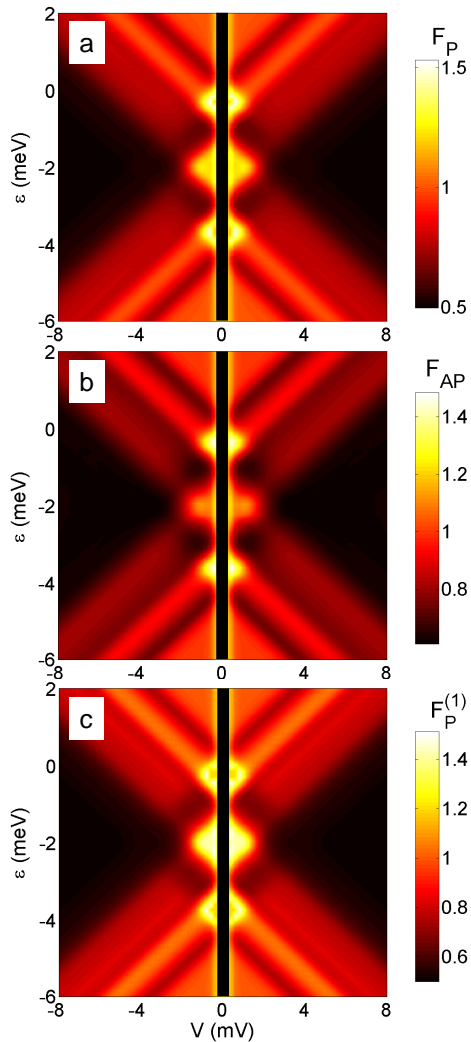


FIG. 6: (Color online) The total Fano factor in the parallel (a) and antiparallel (b) magnetic configurations as a function of the bias voltage V and the position of the dots' levels ε for parameters the same as in Fig. 2. Part (c) presents the Fano factor in the parallel configuration calculated in the first-order approximation. Because the Fano factor is divergent for $|eV| \lesssim k_B T$, this transport regime is denoted with a thick black line.

tiparallel configuration, yielding generally an enhanced Fano factor in the antiparallel configuration as compared to the parallel one. Moreover, we also note that in the Coulomb blockade regime, $\varepsilon = -2$ meV, the shot noise becomes super-Poissonian ($F > 1$) and drops to the sub-Poissonian value ($F < 1$) at the threshold for sequential tunneling, see Fig. 5(d). This super-Poissonian shot noise is associated with bunching of inelastic cotunneling processes through the system.^{54,81} On the other hand, in the case of empty DQD, $\varepsilon = 2$ meV, in the cotunneling regime the current flows due to elastic second-order processes which obey the Poissonian statistics. In this case the shot noise is given by $S = 2e|I|$ and the Fano factor is simply equal to unity, see Fig. 5(h), irrespective

of magnetic configuration of the system. As concerns the sequential tunneling regime, the shot noise is then generally sub-Poissonian, irrespective of the position of the DQD level ε . This indicates the role of correlations in electronic transport, in particular, the Coulomb correlations and charge conservation.⁸⁰ Our results are in qualitative agreement with experimental data on tunneling through vertically coupled self-assembled InAs quantum dots where also super-Poissonian shot noise has been found.¹⁹

Finally, to make the present analysis self-contained, we also show the bias and gate voltage dependence of the total Fano factor for the parallel and antiparallel magnetic configuration, see Fig. 6(a) and (b), respectively. In addition, for comparison, the Fano factor calculated by taking into account only first-order tunneling processes is depicted in Fig. 6(c). The black lines around the zero bias, $|eV| \lesssim k_B T$, mark the transport regime where the Fano factor is divergent due to finite thermal noise. The different behavior of the shot noise is now clearly visible. In the Coulomb blockade regime the noise is super-Poissonian, in the cotunneling regime when the DQD is either empty or fully occupied (current is mediated by elastic cotunneling) the shot noise is Poissonian, and in the sequential tunneling regime the noise drops to sub-Poissonian value.

B. Asymmetric double quantum dots: Pauli spin blockade

By applying a gate voltage to each quantum dot, it is possible to tune the dot levels separately. So far, we have considered the case of symmetric DQD, i.e. when $\varepsilon_1 = \varepsilon_2$. In this situation the transport characteristics were symmetric with respect to the bias reversal. This is however not the case for $\varepsilon_1 \neq \varepsilon_2$, where the current becomes asymmetric with respect to the bias reversal, leading to the Pauli spin blockade and negative differential conductance, as observed experimentally.^{6,8} In the following, assuming realistic parameters of the double quantum dot system, we analyze transport properties in the regime where the Pauli spin blockade effects are visible.

The mechanism leading to the spin blockade was theoretically discussed by Fransson *et al.*¹⁵ and Muralidharan *et al.*¹⁸ These considerations were however restricted only to the first-order tunneling processes, which dominate the current out of the blockade regime. As shown experimentally by Ono *et al.*,⁶ in the spin blockade regime there is a finite leakage current, which cannot be explained within the sequential tunneling approximation. To explain the existence of this leakage, it was proposed that non-zero current in the Pauli blockade is associated with spin-flip processes induced by hyperfine interaction.¹⁷ In the following, we show that the leakage current results just from the interplay between different intrinsic tunneling processes driving the current. The hyperfine interaction, or coupling to a phonon bath, may, of course, increase the

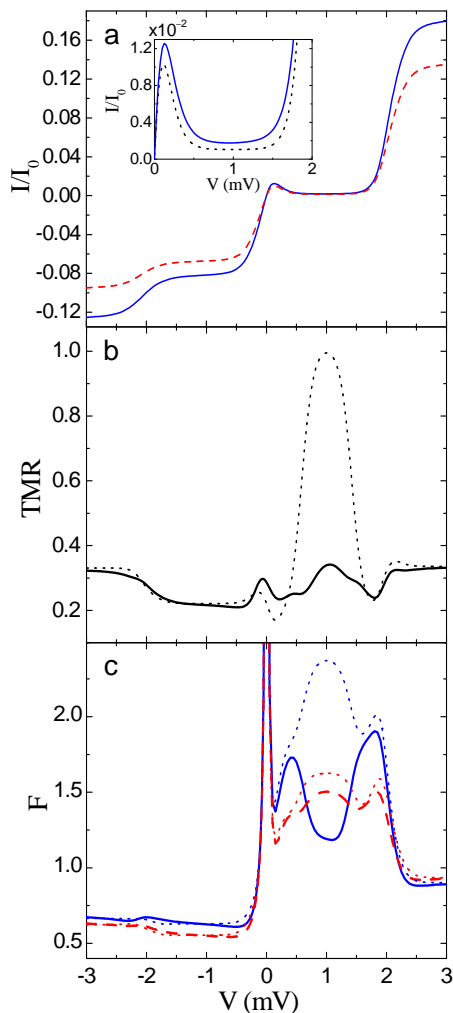


FIG. 7: (Color online) The current (a) and Fano factor (c) in the parallel (solid) and antiparallel (dashed) magnetic configurations as well as the TMR (b) as a function of the bias voltage for DQD coupled in series. The parameters are: $k_B T = 0.05$ meV, $\varepsilon_1 = -1$ meV, $\varepsilon_2 = -2$ meV, $\Delta = 3$ meV, $U = 2$ meV, $U' = 1$ meV, $t = 0.05$ meV, where Δ is the level spacing in each dot. The other parameters are the same as in Fig. 2. The inset in part (a) displays the current in the parallel magnetic configuration in the Pauli spin blockade regime. The dotted lines correspond to the first-order calculation.

leakage, but is not necessary for the observation of a finite current in the Pauli spin blockade regime.

When the DQDs levels are detuned, $\varepsilon_2 < \varepsilon_1$, and once the first and second dot become singly occupied, the current may be suppressed in some range of the bias voltage. This is associated with the full occupation of two-electron triplet states of the DQD.¹⁵ The Pauli spin blockade may be lifted when the applied bias voltage admits another (excited) charge states to participate in transport. On the other hand, when the voltage is reversed, it is energetically allowed that the electron from the first dot tunnels to the left lead and then another electron from the right lead enters the DQD, lifting the Pauli spin blockade.

This can be seen in Fig. 7 where we present the bias voltage dependence of the current, Fano factor and the TMR effect. In order to make the calculations more realistic and to allow for excited states of the system, we have now taken into account four different orbital levels, two in each dot. Such system is described by straightforward extension of the hamiltonian, Eq. (2), where the level spacing in the dots is described by the parameter Δ . First of all, one can see that the transport characteristics are asymmetric with respect to the bias reversal. This is associated with the fact that by detuning the DQDs levels the symmetry of transition rates between the left and right leads has been broken. Furthermore, for positive bias voltage the current is suppressed in a broad range of the bias voltage ($0 < eV < U$) due to the full occupation of the triplet states, while for negative bias the Pauli spin blockade is lifted. In addition, the blockade can also be lifted when the positive bias voltage is increased further, $eV > U$, so that tunneling through the second level of the second dot is allowed, see Fig. 7(a).

In the inset of Fig. 7(a) we show the current in the parallel configuration just in the spin blockade regime. For comparison, we also display the current calculated within the sequential tunneling approximation. One can see that the sequential current is suppressed as compared to the total current (calculated taking into account cotunneling processes). The suppression of the sequential current is generally governed by the ratio $2t/|\varepsilon_2 - \varepsilon_1|$.¹⁵ When $2t/|\varepsilon_2 - \varepsilon_1| \ll 1$, the occupation of the two-electron triplet states approaches unity and the first-order current becomes fully blocked. However, the second-order processes are still allowed, leading to a finite leakage current in the spin blockade regime. One can distinguish different contributions coming from cotunneling:

- (i) The double-barrier elastic second-order processes which contribute directly to the current.
- (ii) The double-barrier spin-flip cotunneling which contributes to the current and reduces the occupation of the triplet state, this way opening the DQD for the sequential tunneling.
- (iii) The single-barrier spin-flip cotunneling which does not contribute directly to the current but flips the spin in the DQD and allows the sequential processes to occur.

As a consequence, in the Pauli spin blockade regime the current flows due to cotunneling and spin-flip cotunneling-assisted sequential tunneling. The key role is played by the spin-flip processes which decrease the occupation of the two-electron triplet states and lead to a finite occupation of singlet states. The importance of the spin-flip processes in explanation of the finite leakage current has been invoked in Ref. [17]. The leakage was there associated with spin-flip processes induced by hyperfine interaction through the Overhauser effect. Here, we show that the leakage results just from the interplay between different tunneling processes, i.e. just from the pure nature of tunneling processes. We also note that the effects of cotunneling are rather independent of the material from which the dots are built, unlike the Overhauser

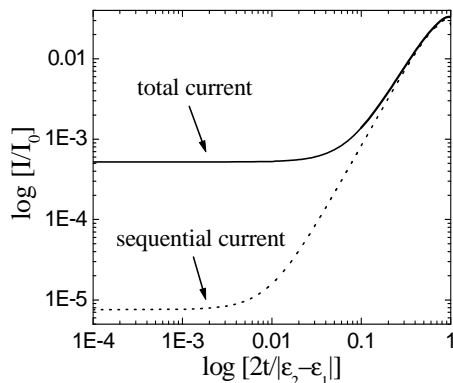


FIG. 8: The total (sequential plus cotunneling) current (solid line) and the sequential current (dotted line) in the parallel configuration as a function of the hopping between the two dots calculated in the middle of the Pauli spin blockade regime, $V = 1$ mV. The parameters are the same as in Fig. 7. The dependence of the current on $2t/|\varepsilon_2 - \varepsilon_1|$ in the antiparallel configuration is qualitatively similar.

field.⁸² Thus, for example, in GaAs DQDs the leakage current in the Pauli spin blockade would be associated with both cotunneling and hyperfine contributions, while in carbon nanotube DQDs it would be mainly due to cotunneling. Furthermore, as shown in experiments by Ono and Tarucha,⁸³ who studied the dependence of the leakage current on the applied magnetic field, the hyperfine interaction starts to play a role at certain finite in-plane magnetic fields, at which the nuclei become polarized, leading to a sudden jump of the leakage current as a function of magnetic field. This suggests that the main contribution to the current in the spin blockade regime in the absence of magnetic field may come from cotunneling. In the weak coupling regime, typical values of the dot-lead coupling strength Γ are of the order of μeV ,⁸⁴ which gives the leakage current of the order of $10^{-3}I_0 \approx 1$ pA (see Fig. 8), in agreement with experimental results.⁸³ Finally, we notice that to explain the jump in the leakage current when sweeping magnetic field, besides cotunneling, one also has to include the hyperfine interaction. Nevertheless, this goes beyond the scope of the present paper.

In Fig. 8 we present the logarithmic dependence of the sequential and total currents in the parallel configuration on the hopping parameter t . It is clearly visible that for $2t/|\varepsilon_2 - \varepsilon_1| \ll 1$, the sequential current is smaller by two orders of magnitude than the total current. On the other hand, when $2t/|\varepsilon_2 - \varepsilon_1| \approx 1$, the sequential current becomes of the same order as the total current, but still, noticeably, the total current is larger than that calculated using only the first-order tunneling processes. The saturation of the two currents for $2t/|\varepsilon_2 - \varepsilon_1| \ll 1$, see Fig. 8, is associated with a finite temperature. However, because sequential tunneling depends exponentially on temperature while cotunneling only algebraically, at lower T the difference between the two currents would be

even more pronounced. The dependence of the current in the antiparallel configuration is qualitatively similar to the one shown in Fig. 8. We also note that generally the above mentioned mechanism responsible for the leakage current does not depend on whether the leads are made of ferromagnetic or nonmagnetic material.

The TMR as a function of the bias voltage is displayed in Fig. 7(b). One can see that the TMR calculated using the first-order processes and that calculated taking into account cotunneling are generally similar, except for the Pauli spin blockade regime. In this transport regime the sequential TMR is much overestimated. To understand this behavior we note again that the blockade results from the full occupation of DQD's triplet states. The probability is equally distributed between the three components of the triplet in the parallel configuration. However, in the antiparallel configuration, it turns out that the charge is mainly accumulated in the $S_z = 1$ component of the triplet. As a consequence, in the parallel configuration all the three components of the triplet participate in transport, while in the antiparallel configuration only one. Because the sequential current in the blockade regime is mainly associated with thermal fluctuations, the difference in the number of states relevant for transport leads to large sequential TMR in blockade regime. This difference also gives rise to the corresponding difference between Fano factors calculated in the sequential tunneling approximation, see the dotted curves in Fig. 7(c). The shot noise is then super-Poissonian and larger in the parallel configuration. However, as pointed above, the leakage current in the Pauli spin blockade regime is due to cotunneling and cotunneling-assisted sequential tunneling processes. The total current flows not only due to thermal fluctuations but due to correlated tunneling through virtual states of the DQD. This fact generally decreases the current fluctuations and the difference between the two magnetic configurations. As a result, the total TMR and Fano factor become suppressed as compared to the sequential tunneling results, see Fig. 7(b) and (c), respectively. In addition, we also notice that, irrespective of the magnetic configuration of the system, the shot noise is super-Poissonian in the spin blockade regime and drops to sub-Poissonian value out of the blockade regime, see Fig. 7(c). The super-Poissonian shot noise is generally due to bunching of spin-flip cotunneling and cotunneling-assisted sequential tunneling processes.

V. DOUBLE QUANTUM DOTS COUPLED IN PARALLEL

In this section we analyze the spin-polarized transport through double quantum dots coupled in parallel. This geometry can be realized by setting $\Gamma_{rj} \equiv \Gamma/2$, for $r = L, R$ and $j = 1, 2$, see Fig. 1. We note that in the case of negligible hopping between the two quantum dots, $t \rightarrow 0$, the behavior of the DQD system resembles that of a

single multi-level quantum dot. The problem of spin-dependent transport through multi-level quantum dots has been addressed very recently in Ref. [54] and will not be considered here.

In Fig. 9 we present the density plots of the differential conductance and Fano factor in the parallel configuration as well as of the TMR effect as a function of the bias and gate voltages. The behavior of the conductance and the shot noise in the antiparallel configuration is qualitatively similar as in the parallel configuration, therefore, it is not shown here. The information about the difference in transport in the two magnetic alignments is contained in the TMR, whose magnitude reflects the asymmetry in tunneling processes when the leads are parallel or antiparallel to each other.

The differential conductance, shown in Fig. 9(a), displays characteristic Coulomb diamonds. Because the internal energy structure of the DQD is generally the same as in the case of DQD coupled in series, the differential conductances are qualitatively similar, see Figs. 2(a) and 9(a). The main difference is that in the case of parallel DQDs the level of each dot is coupled both to the left and right leads, which generally results in an enhanced conductance for parallel DQDs as compared to DQDs coupled in series. Similarly the TMR shown in Fig. 9(b), its bias and gate voltage dependence is only slightly modified as compared to Fig. 3(a). Again, the linear TMR exhibits a strong dependence on the occupation number of the DQD, with TMR given by the Julliere formula for empty and fully occupied double quantum dot, and is much suppressed in other transport regimes due to spin-flip cotunneling. In the Coulomb blockade regime, the transport properties are mainly conditioned by the spin-flip cotunneling, which gives a dominant contribution to the current. Furthermore, the bunching of spin-flip cotunneling in the Coulomb blockade regime leads to super-Poissonian shot noise, see Fig. 9(c). The super-Poissonian shot noise is however more pronounced in Coulomb blockade regimes with an odd number of electrons in the double dot. On the other hand, for voltages above the threshold for sequential tunneling, the shot noise becomes sub-Poissonian, with the Fano factor approaching $1/2$.

Summing up, we notice that generally in the weak coupling regime the effect of different geometries of the double dot system leads only to qualitative difference in transport properties. The main difference is in the magnitude of conductance – for parallel DQDs it is roughly two times larger than for serial DQDs. This is contrary to the strong coupling regime where, for example, in the parallel geometry the orbital Kondo phenomenon arises due to the interference effects, while for DQDs coupled in series the orbital Kondo effect is destroyed.⁸⁵ Finally, we also note that in the case of detuned levels, $|\varepsilon_2 - \varepsilon_1| \gg 0$, transport properties of double quantum dots coupled in parallel are qualitatively similar to those of single multi-level quantum dots.⁵⁴

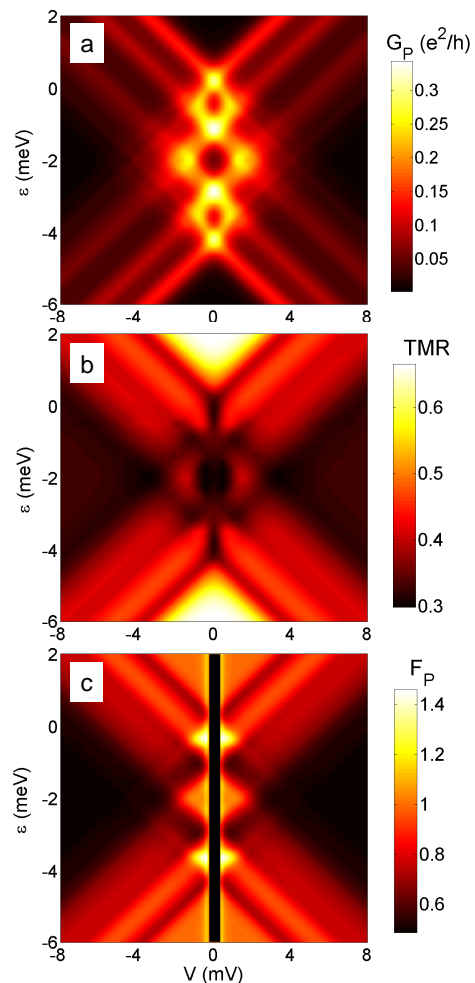


FIG. 9: (Color online) The differential conductance (a) and Fano factor (c) in the parallel magnetic configuration, and the TMR (b) as a function of the bias voltage V and the position of the dots' levels $\varepsilon \equiv \varepsilon_1 = \varepsilon_2$ for double quantum dots coupled in parallel. The parameters are the same as in Fig. 2 with $\Gamma_{rj} \equiv \Gamma/2$, for $r = L, R$, $j = 1, 2$, and $\Gamma = 0.1$ meV. The transport regime where the Fano factor is divergent is marked with a thick black line.

VI. T-SHAPED DOUBLE QUANTUM DOTS

An interesting situation occurs when only one of the two quantum dots is coupled to external leads, while the other one is decoupled. In such T-shaped systems transport takes place through the molecular states of the double dot, although only the first dot is directly coupled to the leads. This may lead to new transport behavior, especially to a large super-Poissonian shot noise and an enhanced TMR, as we show in the sequel.

In Fig. 10 we present the current, differential conductance, the TMR and the Fano factor as a function of the bias voltage for the case when the first dot is coupled to the leads while the second dot is decoupled. Spin-dependent transport through single quantum dots have already been extensively studied. However, the hopping

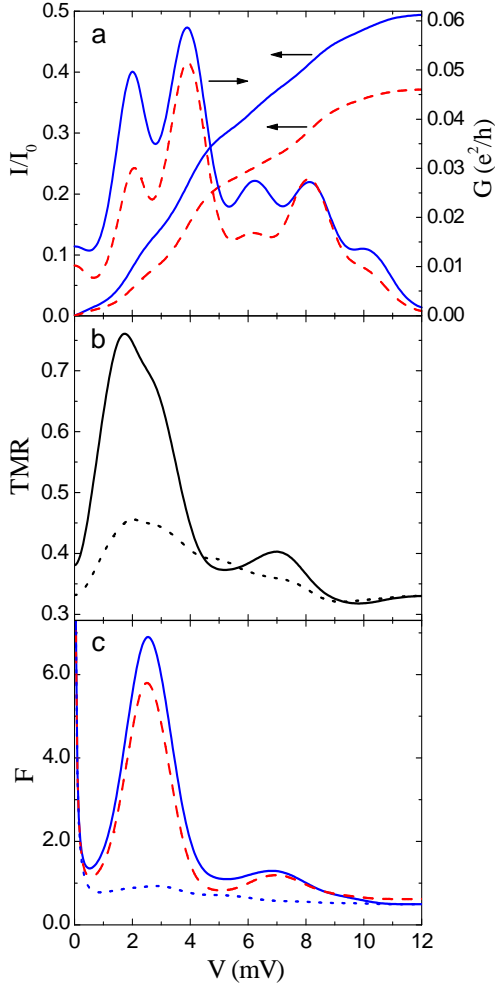


FIG. 10: (Color online) The bias dependence of the current and differential conductance (a), the TMR (b), and the Fano factor (c) in the parallel (solid line) and antiparallel (dashed line) configurations for T-shaped double quantum dots. The parameters are: $\Gamma_{r1} \equiv \Gamma/2$, and $\Gamma_{r2} = 0$ for $r = L, R$, with $\Gamma = 0.1$ meV, and $\varepsilon_1 = 1$ meV, $\varepsilon_2 = 0$ meV, $k_B T = 0.18$ meV, $U = 2$ meV, $U' = 1$ meV, $t = 0.2$ meV, and $p = 0.5$. The dotted curves present the TMR (b) and the Fano factor in the parallel configuration (c) calculated for $\Gamma_{r2} = \Gamma_{r1}$.

t between the two dots may modify the transport properties significantly, giving rise to novel behavior. First of all, we note that due to the finite t , transport takes place through molecular states of the double dot. This in turn leads to additional steps in the i - v curves and peaks in the differential conductance, see Fig. 10(a), as compared to tunneling through one single-level quantum dots, where for spin-degenerate level the current exhibits only two steps. The difference between the currents in the parallel and antiparallel configurations gives rise to the TMR which is shown in Fig. 10(b). The TMR displays an oscillatory-like behavior with increasing the bias voltage. In addition, at the threshold for sequential tunneling, the TMR becomes increased above the Julliere TMR.³⁷ This result is rather counterintuitive, as the Julliere TMR is

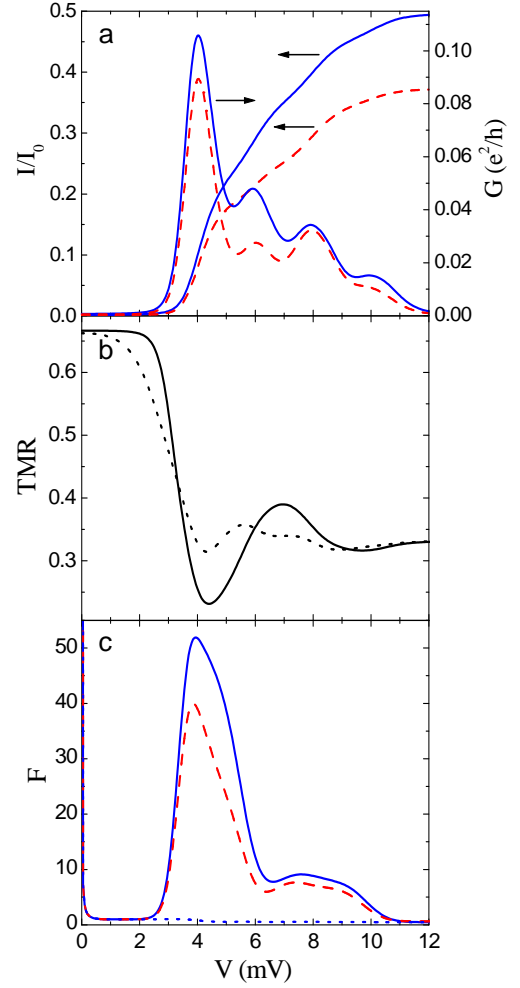


FIG. 11: (Color online) The bias dependence of the current, differential conductance (a), TMR (b) and the Fano factor (c) in the parallel (solid line) and antiparallel (dashed line) configurations. The parameters are the same as in Fig. 10 with $\varepsilon_2 = -4$ meV. The dotted curves present the TMR (b) and the Fano factor in the parallel configuration (c) calculated for $\Gamma_{r2} = \Gamma_{r1}$.

characteristic of a single ferromagnetic tunnel junction and one would expect that an additional object (quantum dot) between the leads should decrease the TMR. This was shown for single quantum dots with spin degenerate levels and symmetric couplings to the leads where the TMR was found to take at most the Julliere value.⁴³ In principle, the TMR can be enhanced above the Julliere value when only one spin component of the dot takes part in transport. Such spin selection may be achieved upon applying an external magnetic field or due to finite exchange interaction between spins in the dot.^{46,86} In the case of T-shaped DQDs, we find that the enhancement of the TMR is associated with increased occupation of the second dot in the antiparallel configuration, as compared to the parallel. Because the second dot is decoupled from the leads, this increases the difference between the current in the two configurations, yielding the TMR larger

than the Julliere value. In addition, finite occupation of the decoupled dot also leads to large current fluctuations, as the rate for tunneling between the second dot is much slower than that for tunneling between the first dot and the leads. This in turn gives rise to super-Poissonian shot noise, as displayed in Fig. 10(c). The super-Poissonian shot noise is present in both magnetic configurations. It is also slightly larger in the parallel configuration than in the antiparallel one, which is due to an additional contribution to the noise coming from spin-dependent tunneling between the dots and the leads.⁵⁴ We note that the super-Poissonian shot noise in T-shaped dots has also been reported in the case of nonmagnetic leads.⁸⁷ The two dots were however rather weakly coupled to each other so that no molecular states were formed, contrary to the case considered here.

The enhancement of the TMR above the Julliere value and the large super-Poissonian shot noise are present approximately at the threshold for sequential tunneling. In this transport regime the current is mainly mediated through the charge states of the decoupled dot. The aforementioned effects should therefore become washed out if there were a finite coupling between the second dot and the leads. This is shown in Fig. 10(b) and (c) where we depict the TMR and Fano factor in the parallel configuration calculated for $\Gamma_{r2} = \Gamma_{r1}$ (see the dotted curves in Fig. 10). The TMR larger than the Julliere TMR accompanied by super-Poissonian shot noise is thus an indication that transport takes place through quantum dot coupled to another dot, which is not connected to the leads directly.

Figure 11 displays the bias dependence of the current, TMR and the Fano factor calculated in the case when at equilibrium the second dot is fully occupied while the first dot is empty. At low bias voltage, the system is in the Coulomb blockade and the double dot is occupied with two electrons in the second dot with unit probability. The current flows then only due to elastic cotunneling processes. This gives rise to the Julliere TMR and Poissonian shot noise, see Fig. 11(b) and (c). With increasing the bias voltage, close to the threshold for sequential tunneling, the occupation of the second dot is slightly lowered at the cost of a finite occupation of another states. This opens the system for the cotunneling-assisted sequential and sequential tunneling processes. Nevertheless, because the double dot is still mainly occupied by two electrons on the decoupled dot, this gives rise to extremely large current fluctuations and Fano factors, see Fig. 11(c). This super-Poissonian shot noise can be considerably reduced once the second dot becomes coupled to the leads, see the dotted curve in Fig. 11(c).

Finally, in Fig. 12 we present the differential conductance in the parallel configuration and the TMR as a function of the bias voltage and the position of the second dot level. The Coulomb blockade regimes are clearly visible in Fig. 12(a), whereas the different behavior of the TMR depending on the transport regime is presented in Fig. 12(b).

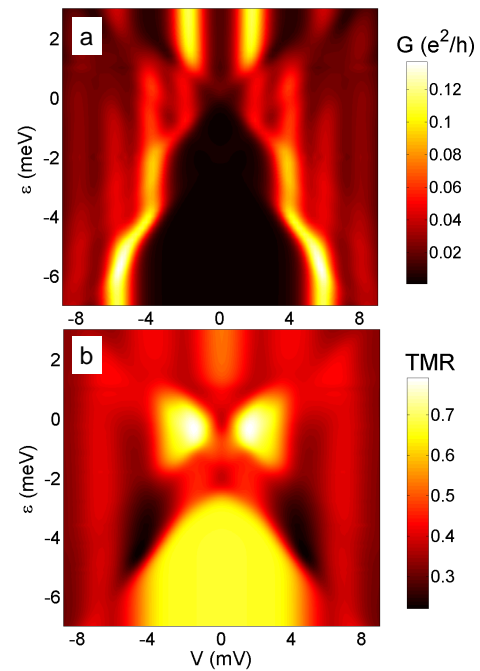


FIG. 12: (Color online) The differential conductance (a) in the parallel magnetic configuration, and the TMR (b) as a function of the bias voltage V and the position of the second dot level $\varepsilon \equiv \varepsilon_2$ for T-shaped double quantum dots. The parameters are the same as in Fig. 10.

VII. CONCLUSIONS

We have analyzed the spin-dependent transport through systems built of two strongly coupled quantum dots which are weakly connected to external ferromagnetic leads. The considerations were based on the real-time diagrammatic technique which allowed us to determine transport properties in the sequential and cotunneling regimes in a fully systematic way. In particular, we have analyzed the current, differential conductance, shot noise and the TMR for different geometries of the double dot system, including the serial and parallel couplings, as well as the T-shaped systems. We have also discussed the main differences in transport characteristics corresponding to different DQDs geometries, which may be helpful in determining the geometry of coupled quantum dots in experiments.

In the case of double quantum dots coupled in series, we have found an interesting dependence of the TMR on the occupation number of the DQD. Furthermore, the super-Poissonian shot noise in the Coulomb blockade regimes have been observed. On the other hand, when the levels of the DQD were detuned, transport characteristics revealed the Pauli spin blockade effects. We have shown that the leakage current, observed experimentally in the blockade regime,⁶ results from the interplay of cotunneling processes which flip the spin in the DQD and make the sequential tunneling possible. Thus, the current in the spin blockade flows due to cotunneling and spin-

flip cotunneling-assisted sequential tunneling processes. This mechanism is associated with pure nature of tunneling processes and is thus relevant for both nonmagnetic and ferromagnetic leads. In addition, we have also shown that the shot noise in the Pauli spin blockade regime becomes super-Poissonian, while outside the blockade it is sub-Poissonian.

For double quantum dots coupled in parallel, transport characteristics were found to be qualitatively similar to those in the case of DQDs coupled in series. The main difference is in the magnitude of conductance – for parallel DQDs it is roughly two times larger than for serial DQDs.

In addition, we have also analyzed the case when the first quantum dot is coupled to the leads while the second one is completely decoupled. In such T-shaped systems we have found a large super-Poissonian shot noise at the threshold for sequential tunneling and the TMR enhanced above the Julliere value. These effects are associated with an increased occupation of the decoupled quantum dot, and become washed out once there is a finite coupling between the second dot and the leads. Thus, the enhanced TMR together with large super-Poissonian shot noise may be an indication that transport takes place through quantum dot which is side-coupled to another

dot disconnected from the leads.

Acknowledgments

We acknowledge fruitful discussions with J. Barnaś. This work was supported by the Foundation for Polish Science and, as part of the European Science Foundation EUROCORES Programme SPINTRA, by funds from the Ministry of Science and Higher Education as a research project in years 2006-2009.

APPENDIX A: DETAILS OF NUMERICAL CALCULATIONS

In order to calculate the transport properties in the sequential and cotunneling regimes, it is necessary to find the elements of the respective first-order and second-order self-energy matrices. This can be done using the respective diagrammatic rules.^{43,75,76} Here, as an example, we present the contribution coming from $W_{\chi(N),\chi'(N)}^{(2)}$ where N is the charge state of the double dot. It is given by

$$\begin{aligned}
W_{\chi(N),\chi'(N)}^{(2)} = & -2\pi \sum_{r,r'} \sum_{j,j'} \sum_{\sigma,\sigma'} \sum_{\chi''} \left\{ |\langle \chi | U^\dagger d_{j\sigma} U | \chi'' \rangle|^2 |\langle \chi'' | U^\dagger d_{j'\sigma'}^\dagger U | \chi' \rangle|^2 \left[\gamma_{rj}^{\sigma+}(\varepsilon_{\chi''} - \varepsilon_\chi) B_{2r'j'}^{\sigma'-}(\varepsilon_{\chi''} - \varepsilon_{\chi'}) \right. \right. \\
& + \gamma_{r'j'}^{\sigma'+}(\varepsilon_{\chi''} - \varepsilon_{\chi'}) B_{2rj}^{\sigma+}(\varepsilon_{\chi''} - \varepsilon_\chi) - B_{2rj'j'}^{\sigma+\sigma'-}(\varepsilon_{\chi''} - \varepsilon_\chi, \varepsilon_{\chi'} - \varepsilon_\chi) \Big] \\
& + |\langle \chi | U^\dagger d_{j\sigma}^\dagger U | \chi'' \rangle|^2 |\langle \chi'' | U^\dagger d_{j'\sigma'} U | \chi' \rangle|^2 \left[\gamma_{rj}^{\sigma-}(\varepsilon_\chi - \varepsilon_{\chi''}) B_{2r'j'}^{\sigma'+}(\varepsilon_{\chi'} - \varepsilon_{\chi''}) \right. \\
& + \gamma_{r'j'}^{\sigma'+}(\varepsilon_{\chi'} - \varepsilon_{\chi''}) B_{2rj}^{\sigma-}(\varepsilon_\chi - \varepsilon_{\chi''}) - B_{2rj'j'}^{\sigma-\sigma'+}(\varepsilon_\chi - \varepsilon_{\chi''}, \varepsilon_\chi - \varepsilon_{\chi'}) \Big] \\
& + \sum_{\chi'''} \langle \chi | U^\dagger d_{j\sigma}^\dagger U | \chi''' \rangle \langle \chi''' | U^\dagger d_{j'\sigma'} U | \chi' \rangle \langle \chi | U^\dagger d_{j'\sigma'} U | \chi'' \rangle \langle \chi'' | U^\dagger d_{j\sigma}^\dagger U | \chi' \rangle \times \\
& \frac{2}{\varepsilon_\chi + \varepsilon_{\chi'} - \varepsilon_{\chi''} - \varepsilon_{\chi'''}} \left[B_{1rj'j'}^{\sigma-\sigma'+}(\varepsilon_{\chi''} - \varepsilon_{\chi'}, \varepsilon_\chi - \varepsilon_{\chi'}) - B_{1rj'j'}^{\sigma-\sigma'+}(\varepsilon_\chi - \varepsilon_{\chi''}, \varepsilon_\chi - \varepsilon_{\chi'}) \right] \Big\}, \quad (A1)
\end{aligned}$$

where $\gamma_{rj}^{\sigma\pm}(\varepsilon) = \Gamma_{rj}^\sigma f^\pm(\varepsilon - \mu_r)/(2\pi)$, with f^+ being the Fermi distribution function, $f^- = 1 - f^+$, μ_r denoting the electrochemical potential of the lead r , and

$$\begin{aligned}
B_{2rj}^{\sigma\pm}(\varepsilon) &= \int d\omega \frac{\gamma_{rj}^{\sigma\pm}(\omega)}{(\omega - \varepsilon)^2}, \\
B_{\eta r j r' j'}^{\sigma\pm\sigma'\mp}(\varepsilon, \varepsilon') &= \int d\omega \gamma_{rj}^{\sigma\pm}(\omega) \gamma_{r'j'}^{\sigma'\mp}(\omega - \varepsilon') \frac{1}{(\omega - \varepsilon)^\eta}.
\end{aligned}$$

We note that having found all the first-order and second-order self-energy matrices, we are in principle able to

calculate transport through arbitrary number of different orbital levels coupled to each other and to external leads in an arbitrary way. As far as numerical details are concerned, for systems consisting of larger number of orbital levels, in calculations we make use of the block structure of the initial Hamiltonian in the charge space, and perform unitary transformation of the Hamiltonian and the relevant local operators for each block separately. In addition, we also store the respective matrix elements in blocks labelled by charge quantum numbers.

-
- * Electronic address: weymann@amu.edu.pl
- ¹ F. R. Waugh, M. J. Berry, D. J. Mar, R. M. Westervelt, K. L. Campman, and A. C. Gossard, Phys. Rev. Lett. **75**, 705 (1995).
 - ² J. J. Palacios and P. Hawrylak, Phys. Rev. B **51**, 1769 (1995).
 - ³ R. H. Blick, R. J. Haug, J. Weis, D. Pfannkuche, K. v. Klitzing, and K. Eberl, Phys. Rev. B **53**, 7899 (1996).
 - ⁴ H. Imamura, H. Aoki, and P. A. Maksym, Phys. Rev. B **57**, R4257 (1998).
 - ⁵ R. Ziegler, C. Bruder, and H. Schoeller, Phys. Rev. B **62**, 1961 (2000).
 - ⁶ K. Ono, D. G. Austing, Y. Tokura, and S. Tarucha, Science **297**, 1313 (2002).
 - ⁷ W. G. van der Wiel, S. De Franceschi, J. M. Elzerman, T. Fujisawa, S. Tarucha, and L. P. Kouwenhoven, Rev. Mod. Phys. **75**, 1 (2003).
 - ⁸ H. W. Liu, T. Fujisawa, T. Hayashi, and Y. Hirayama, Phys. Rev. B **72**, 161305(R) (2005).
 - ⁹ V. N. Golovach and D. Loss, Phys. Rev. B **69**, 245327 (2004).
 - ¹⁰ D. T. McClure, L. DiCarlo, Y. Zhang, H.-A. Engel, C. M. Marcus, M. P. Hanson, and A. C. Gossard, Phys. Rev. Lett. **98**, 056801 (2007).
 - ¹¹ B. Wunsch, M. Braun, J. König, and D. Pfannkuche, Phys. Rev. B **72**, 205319 (2005).
 - ¹² M. R. Gräber, W. A. Coish, C. Hoffmann, M. Weiss, J. Furer, S. Oberholzer, D. Loss, and C. Schönenberger, Phys. Rev. B **74**, 075427 (2006).
 - ¹³ E. Cota, R. Aguado, and G. Platero, Phys. Rev. Lett. **94**, 107202 (2005).
 - ¹⁴ B. L. Hazelzet, M. R. Wegewijs, T. H. Stoof, and Yu. V. Nazarov, Phys. Rev. B **63**, 165313 (2001).
 - ¹⁵ J. Fransson, M. Rasander, Phys. Rev. B **73**, 205333 (2006).
 - ¹⁶ J. Fransson, Nanotechnology **17**, 5344 (2006); New J. Phys. **8**, 114 (2006).
 - ¹⁷ J. Inarrea, G. Platero and A. H. MacDonald, Phys. Rev. B **76**, 085329 (2007).
 - ¹⁸ B. Muralidharan and S. Datta, Phys. Rev. B **76**, 035432 (2007).
 - ¹⁹ P. Barthold, F. Hohls, N. Maire, K. Pierz, and R. J. Haug, Phys. Rev. Lett. **96**, 246804 (2006).
 - ²⁰ G. Kießlich, E. Schöll, T. Brandes, F. Hohls, and R. J. Haug, Phys. Rev. Lett. **99**, 206602 (2006).
 - ²¹ J. Aghassi, A. Thielmann, M. H. Hettler, and G. Schön, Phys. Rev. B **73**, 195323 (2006).
 - ²² P. Trocha, J. Barnaś, Phys. Rev. B **76**, 165432 (2007).
 - ²³ I. Weymann, Phys. Rev. B **75**, 195339 (2007).
 - ²⁴ J. N. Pedersen, B. Lassen, A. Wacker, and M. H. Hettler, Phys. Rev. B **75**, 235314 (2007).
 - ²⁵ S. A. Wolf, D. D. Awschalom, R. A. Buhrman, J. M. Daughton, S. von Molnar, M. L. Roukes, A. Y. Chtchelka, and D. M. Treger, Science **294**, 1488 (2001).
 - ²⁶ *Semiconductor Spintronics and Quantum Computation*, ed. by D.D. Awschalom, D. Loss, and N. Samarth (Springer, Berlin 2002).
 - ²⁷ S. Maekawa and T. Shinjo, *Spin Dependent Transport in Magnetic Nanostructures* (Taylor & Francis, New York 2002).
 - ²⁸ I. Zutic, J. Fabian, S. Das Sarma, Rev. Mod. Phys. **76**, 323 (2004).
 - ²⁹ S. Maekawa, *Concepts in Spin Electronics* (Oxford University Press, 2006).
 - ³⁰ R. Aguado and D. C. Langreth, Phys. Rev. Lett. **85**, 1946 (2000).
 - ³¹ R. Lopez, R. Aguado, and G. Platero, Phys. Rev. Lett. **89**, 136802 (2002).
 - ³² J. C. Chen, A. M. Chang, and M. R. Melloch, Phys. Rev. Lett. **92**, 176801 (2004).
 - ³³ D. Loss and D. P. DiVincenzo, Phys. Rev. A **57**, 120 (1998).
 - ³⁴ D. Loss and E. V. Sukhorukov, Phys. Rev. Lett. **84**, 1035 (2000).
 - ³⁵ X. Hu and S. Das Sarma, Phys. Rev. A **61**, 062301 (2000).
 - ³⁶ R. Hanson and G. Burkard, Phys. Rev. Lett. **98**, 050502 (2007).
 - ³⁷ M. Julliere, Phys. Lett. A **54**, 225 (1975).
 - ³⁸ J. Barnaś and A. Fert, Phys. Rev. Lett. **80**, 1058 (1998); S. Takahashi and S. Maekawa, Phys. Rev. Lett. **80**, 1758 (1998).
 - ³⁹ B. R. Buřka, Phys. Rev. B **62**, 1186 (2000).
 - ⁴⁰ W. Rudziński and J. Barnaś, Phys. Rev. B **64**, 085318 (2001).
 - ⁴¹ J. König and J. Martinek, Phys. Rev. Lett. **90**, 166602 (2003).
 - ⁴² M. Braun, J. König, J. Martinek, Phys. Rev. B **70**, 195345 (2004); Phys. Rev. B **74**, 075328 (2006).
 - ⁴³ I. Weymann, J. König, J. Martinek, J. Barnaś, and G. Schön, Phys. Rev. B **72**, 115334 (2005).
 - ⁴⁴ I. Weymann, J. Barnaś, J. König, J. Martinek, and G. Schön, Phys. Rev. B **72**, 113301 (2005).
 - ⁴⁵ S. Braig and P. W. Brouwer, Phys. Rev. B **71**, 195324 (2005).
 - ⁴⁶ I. Weymann, J. Barnaś, Phys. Rev. B **73**, 205309 (2006); Phys. Rev. B **75**, 155308 (2007); Eur. Phys. J. B **46**, 289 (2005); I. Weymann, Europhys. Lett. **76**, 1200 (2006).
 - ⁴⁷ F. M. Souza, J. C. Egues, and A. P. Jauho, Phys. Rev. B **75**, 165303 (2007).
 - ⁴⁸ J. Fransson, Europhys. Lett. **70**, 796 (2005).
 - ⁴⁹ A. Cottet, W. Belzig, and C. Bruder, Phys. Rev. B **70**, 115315 (2004); Phys. Rev. Lett. **92**, 206801 (2004).
 - ⁵⁰ A. Cottet and M.-S. Choi, Phys. Rev. B **74**, 235316 (2006).
 - ⁵¹ J. Martinek, Y. Utsumi, H. Imamura, J. Barnaś, S. Maekawa, J. König, and G. Schön, Phys. Rev. Lett. **91**, 127203 (2003); M.-S. Choi, D. Sanchez, and R. Lopez, Phys. Rev. Lett. **92**, 056601 (2004).
 - ⁵² Y. Utsumi, J. Martinek, G. Schön, H. Imamura, and S. Maekawa, Phys. Rev. B **71**, 245116 (2005).
 - ⁵³ M. Sindel, L. Borda, J. Martinek, R. Bulla, J. König, G. Schön, S. Maekawa, and J. von Delft, Phys. Rev. B **76**, 045321 (2007).
 - ⁵⁴ I. Weymann and J. Barnaś, Phys. Rev. B **77**, 075305 (2008).
 - ⁵⁵ R. Hornberger, S. Koller, G. Begemann, A. Donarini, and M. Grifoni, cond-mat/0712.0757 (unpublished).
 - ⁵⁶ J. R. Petta, A. C. Johnson, C. M. Marcus, M. P. Hanson, and A. C. Gossard, Phys. Rev. Lett. **93**, 186802 (2004).
 - ⁵⁷ A. C. Johnson, J. R. Petta, and C. M. Marcus, M. P. Hanson and A. C. Gossard, Phys. Rev. B **72**, 165308 (2005).
 - ⁵⁸ H. I. Jorgensen, K. Grove-Rasmussen, J. R. Hauptmann, P. E. Lindelof, Appl. Phys. Lett. **89** 232113 (2006).
 - ⁵⁹ S. Sapmaz, C. Meyer, P. Beliczynski, P. Jarillo-Herrero,

- Leo P. Kouwenhoven, Nano Lett. **6** (7), 1350 (2006).
- ⁶⁰ M. R. Gräber, M. Weiss, C. Schönenberger, Semicond. Sci. Technol. **21**, 64 (2006).
- ⁶¹ Y. Chye, M. E. White, E. Johnston-Halperin, B. D. Gerardot, D. D. Awschalom, and P. M. Petroff, Phys. Rev. B **66**, 201301(R) (2002).
- ⁶² H. B. Heersche, Z. de Groot, J. A. Folk, L. P. Kouwenhoven, and H. S. J. van der Zant, A. A. Houck, J. Labaziewicz, and I. L. Chuang, Phys. Rev. Lett. **96**, 017205 (2006).
- ⁶³ L. Y. Zhang, C. Y. Wang, Y. G. Wei, X. Y. Liu, and D. Davidović, Phys. Rev. B **72**, 155445 (2005).
- ⁶⁴ K. Tsukagoshi, B. W. Alphenaar, and H. Ago, Nature **401**, 572 (1999).
- ⁶⁵ B. Zhao, I. Mönch, H. Vinzelberg, T. Mühl, and C. M. Schneider, Appl. Phys. Lett. **80**, 3144 (2002).
- ⁶⁶ A. Jensen, J. R. Hauptmann, J. Nygard, and P. E. Lindelof, Phys. Rev. B **72**, 035419 (2005).
- ⁶⁷ S. Sahoo, T. Kontos, J. Furer, C. Hoffmann, M. Gräber, A. Cottet, and C. Schönenberger, Nature Physics **1**, 102 (2005).
- ⁶⁸ A. N. Pasupathy, R. C. Bialczak, J. Martinek, J. E. Grose, L. A. K. Donev, P. L. McEuen, and D. C. Ralph, Science **306**, 86 (2004).
- ⁶⁹ A. Bernand-Mantel, P. Seneor, N. Lidgi, M. Munoz, V. Cros, S. Fusil, K. Bouzehouane, C. Deranlot, A. Vaures, F. Petroff, and A. Fert, Appl. Phys. Lett. **89**, 062502 (2006).
- ⁷⁰ K. Hamaya, S. Masubuchi, M. Kawamura, T. Machida, M. Jung, K. Shibata, K. Hirakawa, T. Taniyama, S. Ishida, and Y. Arakawa, Appl. Phys. Lett. **90**, 053108 (2007).
- ⁷¹ K. Hamaya, M. Kitabatake, K. Shibata, M. Jung, M. Kawamura, K. Hirakawa, T. Machida, T. Taniyama, S. Ishida, and Y. Arakawa, Appl. Phys. Lett. **91**, 22107 (2007); Appl. Phys. Lett. **91**, 232105 (2007).
- ⁷² K. Hamaya, M. Kitabatake, K. Shibata, M. Jung, M. Kawamura, S. Ishida, T. Taniyama, K. Hirakawa, Y. Arakawa, and T. Machida, Phys. Rev. B **77**, 081302(R) (2008).
- ⁷³ H. Yang, S.-H. Yang, S. S. P. Parkin, Nano Lett. **8**, 340 (2008).
- ⁷⁴ B. R. Bulka and T. Kostyrko, Phys. Rev. B **70**, 205333 (2004).
- ⁷⁵ H. Schoeller and G. Schön, Phys. Rev. B **50**, 18436 (1994); J. König, J. Schmid, H. Schoeller, and G. Schön, Phys. Rev. B **54**, 16820 (1996).
- ⁷⁶ A. Thielmann, M. H. Hettler, J. König, and G. Schön, Phys. Rev. Lett. **95**, 146806 (2005); Phys. Rev. B **68**, 115105 (2003).
- ⁷⁷ D. V. Averin and A. A. Odintsov, Phys. Lett. A **140**, 251 (1989); D. V. Averin and Yu. V. Nazarov, Phys. Rev. Lett. **65**, 2446 (1990).
- ⁷⁸ K. Kang and B. I. Min, Phys. Rev. B **55**, 15412 (1997).
- ⁷⁹ D. V. Averin and Yu. V. Nazarov, in *Single Charge Tunneling*, edited by H. Grabert and M. Devoret (Plenum, New York 1992).
- ⁸⁰ Ya. M. Blanter and M. Büttiker, Phys. Rep. **336**, 1 (2000).
- ⁸¹ E. V. Sukhorukov, G. Burkard, and D. Loss, Phys. Rev. B **63**, 125315 (2001).
- ⁸² R. Hanson, L. P. Kouwenhoven, J. R. Petta, S. Tarucha, L. M. K. Vandersypen, Rev. Mod. Phys. **79**, 1217 (2007).
- ⁸³ K. Ono and S. Tarucha, Phys. Rev. Lett. **92**, 256803 (2004).
- ⁸⁴ A. Kogan, S. Amasha, D. Goldhaber-Gordon, G. Granger, M. A. Kastner, and H. Shtrikman, Phys. Rev. Lett. **93**, 166602 (2004).
- ⁸⁵ A. W. Holleitner, A. Chudnovskiy, D. Pfannkuche, K. Eberl, and R. H. Blick, Phys. Rev. B **70**, 075204 (2004).
- ⁸⁶ I. Weymann and J. Barnaś, J. Phys.: Condens. Matter **19**, 096208 (2007).
- ⁸⁷ I. Djuric, B. Dong, H. L. Cui, Appl. Phys. Lett. **87**, 032105 (2005).